JGR Atmospheres

RESEARCH ARTICLE
10.1029/2021JD036414

Particle-Phase Uptake and Chemistry of Highly Oxygenated Organic Molecules (HOMs) From α-Pinene OH Oxidation

L. Poulain[1], A. Tilgner[1], M. Brüggemann[1,2], P. Mettke[1], L. He[1,3], J. Anders[1,4], O. Böge[1], A. Mutzel[1,5], and H. Herrmann[1,6]

[1]Atmospheric Chemistry Department (ACD), Leibniz Institute for Tropospheric Research (TROPOS), Leipzig, Germany, [2]Now at Bayer AG, CropScience Division, R&D, Environmental Safety, Monheim, Germany, [3]Now at China Railway Construction Corporation (CRCC) development group, Beijing, China, [4]Now at Institute of Chemistry, Martin-Luther-University Halle-Wittenberg, Halle, Germany, [5]Now at Eurofins Institute Dr. Appelt Leipzig GmbH, Leipzig, Germany, [6]School of Environmental Science and Engineering, Shandong University (SDU), Qingdao, China

Abstract Secondary organic aerosol (SOA) forms a major part of the tropospheric submicron particle mass. Still, the exact formation mechanisms of SOA have remained elusive. It is now admitted that highly oxygenated organic molecules (HOMs) can contribute to a large fraction of SOA formation. In this study, we performed a set of chamber experiments to investigate the SOA formation, and the HOMs uptake and processing directly formed by OH-radical initiated oxidation of α-pinene under two different aerosol seed conditions. Numerous HOM compounds were identified using advanced online and offline analytical techniques, and grouped into four classes according to their different uptake behaviors. For the first time, individual HOMs uptake coefficients ranging from 1.1×10^{-2} to 1.5×10^{-1} were experimentally determined and analyzed using a resistance model which considers uptake limitations by individual gas- and/or particle-phase processes. This study demonstrates that the uptake coefficients of HOMs strongly depend on their molar mass and their respective O/C ratio. Results show that aerosol seed composition and phase state affect the initial uptake of HOMs. Furthermore, the study demonstrates that the acidity and/or different seed phase-state can significantly enhance the subsequent uptake through occurring acidity-driven reactions reflected in a reactive behavior, particularly under $(NH_4)HSO_4$ seed conditions, promoting up to 3 times a higher SOA mass formation including the formation of highly oxidized organosulfates (HOOS). Overall, the present study implies that HOMs and their subsequent chemical processing can play an important role in both the early growth of newly formed particles and SOA formation when particle acidity is high.

Plain Language Summary Tropospheric organic aerosol (OA) compounds represent a large part of submicron particulate matter. A big fraction of OA is formed from oxidation of emitted gaseous volatile organic compounds such as α-pinene. Oxidation products are less-volatile compounds that tend to condense on aerosol particles. Recently identified "highly oxygenated organic molecules" (HOMs) are formed by gas-phase autoxidation processes and exhibit very low vapor pressures. Therefore, HOMs are expected to efficiently contribute to secondary organic aerosol (SOA). However, up to now, SOA formation potential of HOMs is still not well described because of lacking experimental investigations and analysis. Consequently, this study aims to investigate the mentioned HOMs partitioning and subsequent SOA formation from the OH-radical initiated oxidation of α-pinene under both Na_2SO_4 and $(NH_4)HSO_4$ aerosol seed conditions through complex chamber experiments. For the first time, individual HOMs uptake coefficients were determined experimentally. Further investigations demonstrated that the uptake coefficients of HOMs strongly depend on their molar mass, as well as on their respective O/C ratio. Finally, the results show that aerosol acidity and/or phase state significantly enhances the HOMs uptake and promotes up to three times higher SOA mass formation under $(NH_4)HSO_4$ seed conditions compared to that under neutral seed conditions.

Key Points:

- Uptake coefficients of numerous highly oxygenated organic molecules (HOMs) were experimentally determined for the first time
- HOMs uptake and secondary organic aerosol formation were significantly enhanced by acidic $(NH_4)HSO_4$ seed
- Highly oxidized organosulfates formation were observed under acidic $(NH_4)HSO_4$ seed conditions

Supporting Information:

Supporting Information may be found in the online version of this article.

Correspondence to:

H. Herrmann,
herrmann@tropos.de

Citation:

Poulain, L., Tilgner, A., Brüggemann, M., Mettke, P., He, L., Anders, J., et al. (2022). Particle-phase uptake and chemistry of highly oxygenated organic molecules (HOMs) from α-pinene OH oxidation. *Journal of Geophysical Research: Atmospheres*, *127*, e2021JD036414. https://doi.org/10.1029/2021JD036414

Received 28 DEC 2021
Accepted 24 JUL 2022

1. Introduction

A substantial fraction of sub-micron tropospheric aerosol particles (20%–90%) consists of organic matter (Jimenez et al., 2009; Q. Zhang et al., 2007). Its formation can be attributed to either direct emission of primary organic aerosol or to reactions of organic compounds in the gas phase followed by condensation and chemical processing leading to secondary organic aerosol (SOA; Ervens et al., 2011). Currently, the total global SOA burden is modeled to range from 0.3 to 2.3 Tg (SOA mass; Hodzic et al., 2016; Pai et al., 2020; Spracklen

et al., 2011; Tsigaridis et al., 2014). However, the total global formation source of SOA is still uncertain with 12–1,820 Tg (SOA mass) yr^{-1} based on models and other estimation approaches (Goldstein & Galbally, 2007; Hallquist et al., 2009; Hodzic et al., 2016; Shrivastava et al., 2015; Spracklen et al., 2011; Tsigaridis et al., 2014; Tsigaridis & Kanakidou, 2018). SOA mass estimations are subject to errors due in part to a lack of knowledge about gaseous precursor compounds and their oxidation processes, which result in low-volatility products.

Highly oxygenated organic molecules (HOMs) have been identified during measurements in both remote forest areas and highly polluted megacities, as well as in chamber experiments studying the oxidation of isoprene, monoterpenes, sesquiterpenes, and structurally related compounds (Berndt et al., 2016, 2015; Bianchi et al., 2019; Brüggemann et al., 2017; Ehn et al., 2012; Huang et al., 2021; Jokinen et al., 2014, 2015; Mutzel et al., 2015; Praplan et al., 2015; Rissanen et al., 2014; Tong et al., 2019; Wang et al., 2021). The constituents of this class of gas-phase oxidation products are characterized by a high proportion of oxygen and are formed on a time scale of seconds, which can only be explained by a fast insertion of oxygen via autoxidation mechanisms (Crounse et al., 2013; Ehn et al., 2014). In the formation of HOMs, peroxyl radicals (RO_2) are driving the autoxidation through intramolecular H-shift, leading to the formation of closed-shell products by uni- or bimolecular termination reactions (Berndt et al., 2019; Jokinen et al., 2014; Rissanen et al., 2014; Vereecken & Nozière, 2020; Wang et al., 2021). The resulting stable products contain a variety of functional groups such as multiple hydroperoxide and/or carbonyl groups. For example, HOMs produced from monoterpene ozonolysis were characterized on the molecular level using online tandem mass spectrometry analyses (Tomaz et al., 2021). Due to the proposed numerous functionalities, it is expected that HOMs have low vapor pressures and should quickly condense on aerosol particles (Ehn et al., 2014). Experimental and model investigations have shown that HOMs from α-pinene ozonolysis can be classified as semi-, low- and extremely low volatile organic compounds (SVOC, LVOC, and ELVOC, respectively) applying the volatility basis set (Donahue et al., 2012; Huang et al., 2021; Jokinen et al., 2015; Tröstl et al., 2016). Accordingly, HOMs can be important gas-phase precursors for the formation of SOA.

First evidence for the condensation and following presence of HOMs in the particulate organic mass was shown in a study by Mutzel et al. (2015) from our laboratory, where HOMs containing carbonyl functions were identified in both gas and particle-phases. A later publication by Krapf et al. (2016) quantified the peroxide content of SOA after HOMs condensation and showed that the particle-phase peroxide products are very labile, confirming the findings of Mutzel et al. (2015). The authors quantified the decomposition of particle-phase HOM hydroperoxide (ROOH) moieties with a first-order decomposition rate constant of 2.6×10^{-4} s^{-1} (Krapf et al., 2016). Moreover, molecules containing multiple peroxide functionalities ($C_{8-10}H_{12-18}O_{4-9}$ monomers and $C_{16-20}H_{24-36}O_{8-14}$ dimers) were identified in α-pinene SOA (X. Zhang et al., 2017). Simultaneous detection of these molecules in the gas phase also provides direct evidence for their gas-to-particle conversion. In addition, Tong et al. (2019) found HOMs in ambient fine particulate matter (PM), which was positively correlated with the formation of radicals in aqueous PM extracts. Recently, Roldin et al. (2019) have developed a near-explicit model which can reproduce the observed new particle formation, HOM gas-phase composition and SOA formation over the boreal forest. Since HOMs are considered to contribute to both particle formation and growth to a large extent (Gatzsche et al., 2018; Kristensen et al., 2020; Kürten et al., 2016; J. Zhao, Ortega, et al., 2013), they might explain two-thirds or even entire SOA mass (Ehn et al., 2014).

Decomposition of hydroperoxide functional groups of HOMs can trigger the formation of reactive species, such as OH radicals, and subsequent particle-phase reactions (Tong et al., 2021), from which highly oxidized organosulfates (HOOS) could be further formed (Mutzel et al., 2015). The particle-phase organosulfate formation from α-pinene oxidation was found to be acid-catalyzed (Duporté et al., 2020). Moreover, online aerosol measurements in a forest of Bavaria (Germany) showed that particulate HOOS followed the diurnal behavior of gas-phase HOMs and strongly correlated with particulate sulfate under high relative humidity (RH) conditions (Brüggemann et al., 2017). Besides the monoterpene-derived HOOS, the isoprene-derived methyltetrol sulfates are considered the most abundant HOOS species with ambient concentration of up to 1 μg m^{-3} (Hettiyadura et al., 2017, 2019). These findings confirm that particle-phase chemistry can play an important role in the formation of such compounds (Brüggemann et al., 2020; Herrmann et al., 2015; Tong et al., 2021). Up to now, the particle-phase partitioning and chemistry of HOMs, especially their uptake behavior, have not been fully understood.

The present study aims to investigate the uptake behavior of HOMs formed by the OH-oxidation of α-pinene. Here, special emphasis is placed on the following: (a) determining uptake coefficients of HOMs experimentally for the first time to the best of our knowledge, (b) identifying limiting uptake sub-processes and (c) investigating

the influence of aerosol seed state and surface acidity on the uptake behavior and the associated SOA yield by combining on-line, off-line and modeling approaches.

2. Materials and Methods

2.1. Aerosol Chamber Experiments

Experiments were performed at the 19 m³ (S/V ratio = 2 m^{-1}) TROPOS Atmospheric Chemistry Department Chamber (ACD-C), which was used in a continuous flow reactor (CFR) mode under atmospherically relevant conditions, giving sufficient time for extended filter sampling and corresponding detailed offline organic analysis. A detailed description of the procedure is given in Mutzel et al. (2015) and a schema of the set-up can be found in Figure S1 in Supporting Information S1. Briefly, α-pinene was stored in a glass bulb with a premix 4.317 mbar in 1,949 mbar helium). A constant flow of 1 mL min^{-1} was sampled from the glass bulb and continuously introduced to the chamber using 105 L min^{-1} compress air carrier gases. Similarly, an H_2O_2/H_2O solution (Th. Geyer, $\geq$ 30%) in a gas saturator was flushed at a flowrate of 150 mL min^{-1} and continuously introduced to the chamber with 105 L min^{-1} compress air carrier gases. Consequently, the total incoming flow of 210 L min^{-1} was balanced by a corresponding outflow of 210 L min^{-1} including the sampling flow of all the connected instrumentation maintaining the total volume of the chamber constant (detailed on the individual flow rates are given Figure S1 in Supporting Information S1). The set-up and mode of operation leads to a renewal of 1% of the chamber volume per minute. OH-radicals were generated by the photolysis of H_2O_2 using UV-lamps (Osram EVERSUN® Super, λ = 300–420 nm). Seed particles were produced by atomizing salt solutions (Table S1 in Supporting Information S1). To reach a steady-state condition inside the chamber, the continuous injection of both α-pinene and H_2O_2 started the day before and concentrations were left to stabilize over the night. The next morning, lamps were turned on starting the oxidation of α-pinene and the HOMs production. The fast OH-production leads to a decrease of 30% of the α-pinene concentration inside the chamber. Again, the system was let stabilized over 4–5 hr to reach a new steady-state level for all species, representing approx. 80% of the initial α-pinene concentration. Although OH concentration was not directly measure, to still give an estimation, the change of the steady-state concentration of α-pinene was used to derive the OH concentration. The steady-state concentration decreased from 10.5 to 8.8 ppbv. Using the rate constant of Gill and Hites (2002) an OH concentration of $7 \pm 3 \times 10^5$ molecules cm^{-3} was calculated. Additionally, using the F0AM model with the MCM3.3.1 for α-pinene associated pathways (Wolfe et al., 2016), a steady-state OH concentration of 2×10^6 molecules cm^{-3} was modeled, which is closed to the value estimated from the experiments. Only when this last steady-state was achieved, the seed particles were injected for 2 min (Figure S2 in Supporting Information S1). As the chamber was running in CFR mode, the seed particles were diluted, while the reactants and reaction products remained constant. Therefore, the organic mass concentration was corrected by normalizing it from the decay of the sulfate mass concentration (see details in Supporting Information S1).

Two types of experiments were carried out (see Table S1 in Supporting Information S1): (a) for experiments on HOMs uptake, reactants were injected constantly, and seed particles were introduced for 2 min. This set of experiments can be divided in two experiments depending on the two types of seeds (neutral: Na_2SO_4, or acidic: $(NH_4)HSO_4$) used, while HOMs reactants (α-pinene and H_2O_2) were kept constant over the entire experimental period. To exclude any possible potential conversion of $(NH_4)HSO_4$ to $(NH_4)_2SO_4$ due to a probable contamination of the chamber with ammonia, the NH_4^+ to SO_4^{2-} ratio from the equivalents of NH_4^+ to SO_4^{2-} measured by the AMS was analyzed (see Figure S3 in Supporting Information S1). (b) This set of experiments was dedicated to offline analysis regarding particle-phase compounds. In order to collect enough material, both reactants and seed particles (at the same concentration as for type A) were injected constantly and filters were sampled over approx. 90 h. For each type B experiment, three PTFE filters (fluorocarbon coated borosilicate glass fiber filter, d = 47 mm, PALLFLEX T60A20, PALL, NY, USA) and one quartz fiber filter (QF I, Micro-quartz fiber filter, d = 47 mm, MK 360, Munktell, Bärenstein, Germany) were loaded by sampling volumes as shown in Table S1 in Supporting Information S1. An overview of the experimental conditions is given in Table S1 in Supporting Information S1 and a critical evaluation of different aerosol sinks is given in Section S1 in Supporting Information S1.

2.2. Instrumentation and Chemical Analysis

A set-up of online and offline instrumentation as well as chemical analysis similar to the study of Mutzel et al. (2015) from our laboratory was used. In brief, the detection of gas-phase HOMs was performed using a NO_3^- chemical ionization atmospheric pressure interface time-of-flight mass spectrometer (NO_3^--CI-APi-TOF-MS Airmodus, Ltd., Tofwerk AG) equipped with a compact-ToF-MS (cToF, Tofwerk AG, sampling flow rate 10 L min^{-1}). As synthetic standards for HOMs are not yet available, the instrument was calibrated with sulfuric acid as widely reported in the literature (e.g., Bianchi et al., 2019; Ehn et al., 2014; Mutzel et al., 2015). However, HOMs are generally assumed to have a lower cluster stability, which would result in an underestimation of the actual gas-phase concentrations. That means, all calculated HOMs concentrations have to be understood as H_2SO_4 equivalents and thus, as lower limits for all the given HOMs concentrations. Particle number-size-distribution was followed using a TROPOS-style mobility particle size spectrometer (MPSS; Wiedensohler et al., 2012) at 1 L min^{-1}, while particle chemical composition was measured by a High-Resolution Time-of-Flight Aerosol Mass Spectrometer (HR-TOF-AMS, Aerodyne Inc., DeCarlo et al., 2006) at 0.080 L min^{-1}. In filter experiments (Type B), filter samplers were collected at 30 L min^{-1}. The collected filters were analyzed for particle-phase HOMs, SOA tracer compounds and organosulfates with high-performance liquid chromatography electrospray ionization coupled to time-of-flight mass spectrometry (HPLC/(−)ESI−TOFMS) and ultra-performance liquid chromatography electrospray ionization coupled to time-of-flight mass spectrometry (UPLC/(−)IMS−QTOFMS), respectively. More details on the analytical analysis can be found in Section S1 in Supporting Information S1.

2.3. Phase State Conditions of the Aerosol Seeds

The aerosol-phase state can influence the uptake behavior of gas-phase compounds to aerosol particles, for example, by affecting the diffusion within particles (Y. Zhang et al., 2018). In this study, the two different seeds, Na_2SO_4 and $(NH_4)HSO_4$ were injected in the CFR at low RH conditions (RH < 5%). Based on the literature knowledge, Na_2SO_4 seed particles are present in a solid state under these dry conditions (see e.g., Gao et al., 2007). Different from this, several studies (see Cziczo et al., 1997 and references therein) found that $(NH_4)HSO_4$ seed particles can still prevail in a non-solid state even under really low humidity conditions. Along the same line, Tang and Munkelwitz (1994) showed that $(NH_4)HSO_4$ aerosol particles often remain liquid when they are exposed to very low water vapor at partial pressure of $p < 10^{-6}$ torr. Therefore, the two seeds used in the present study are most likely characterized by different phase states leading to a different uptake behavior.

Besides the aerosol-phase state also the nature of the aerosol surface, particularly the presence of water which in turn enables the presence of acidity on inorganic seeds, can affect the reactive uptake gas phase compounds by altering surface conversions. From studies using Fourier Transform IR-spectroscopy (e.g., Badger et al., 2006) it is known that even under very low RH (<2%) conditions, small amounts of condensed-phase water may be associated with the particle surface, likely promoting the presence of acidity. Therefore, the present study almost certainly includes two different surface acidity seed regimes, a neutral Na_2SO_4 and acidic $(NH_4)HSO_4$ seed, providing different reactive uptake conditions.

Furthermore, the different seeds are characterized by slightly different size distributions. The initial size distribution of Na_2SO_4 and $(NH_4)HSO_4$ peaks at 70 and 80 nm, respectively. However, at such a diameter, the dynamic shape factor is not influencing the sizing and can be considered to be about 1.0 (see e.g., Alexander et al., 2016). As a consequence, the shape of the different seed particles is not affecting the surface area calculation based on MPSS measurements and thus the uptake coefficient calculation.

3. Results and Discussion

HOMs uptake experiments (Type A) are characterized by different behaviors of HOMs in the gas phase which include a steady-state generation of gas-phase HOMs produced by α-pinene/OH oxidation, followed by the initial uptake directly after the seed injection, as well as the subsequent fast and/or slow recoveries under two different aerosol seed conditions. These different periods are going to be discussed in the following respective sections, while the last section is dedicated to the HOMs chemical composition from filter measurements (Type B).

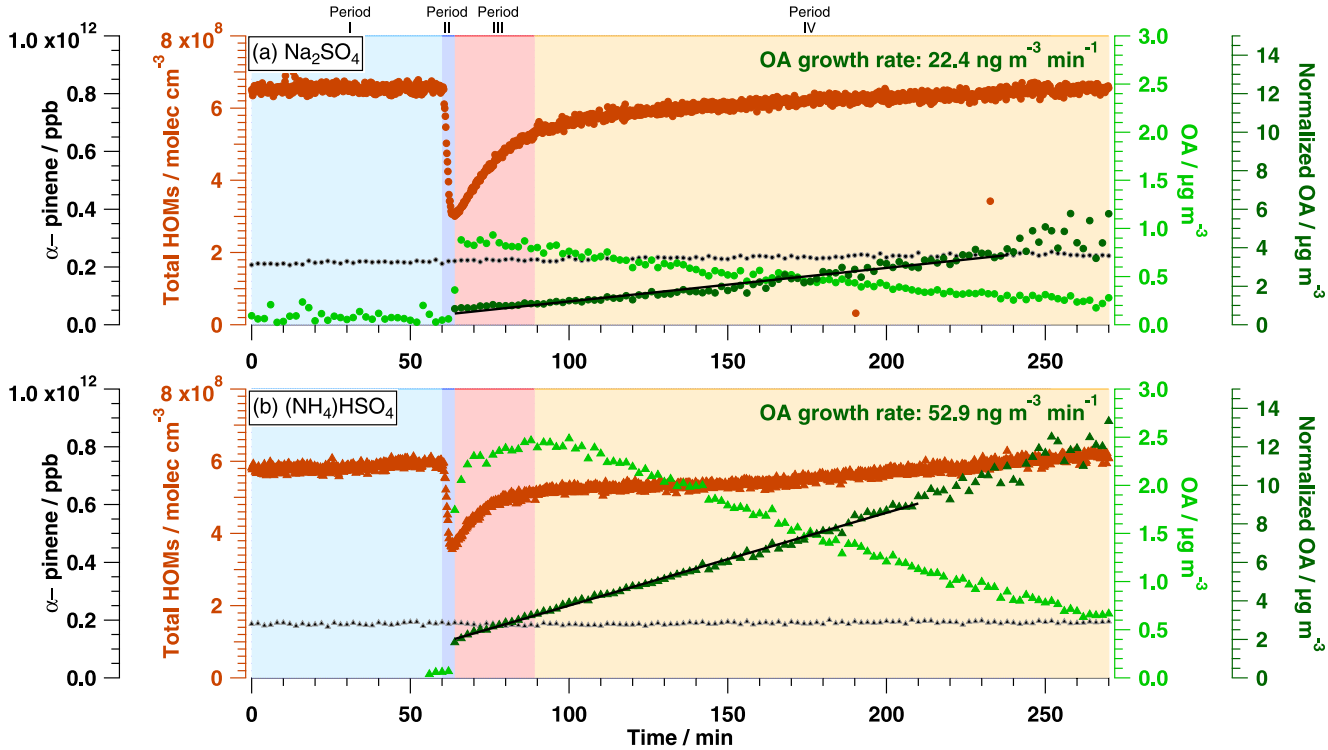

Figure 1. Time courses of concentration of total gas-phase highly oxygenated organic molecules (HOMs; brown), α-pinene (black), organic aerosol (OA, light green), and normalized OA (dark green) in Na_2SO_4 (a) and $(NH_4)HSO_4$ (b) seeds conditions. The shaded range marks the four different periods in both experiments. To consider the dilution of the particles due to the continuous flow reactor (CFR) mode, the organic mass was normalized using the sulfate mass concentration (see details in Supporting Information S1). The rate of the OA mass growth rate has been determined from the slope of the linear fitting of the normalized OA during periods III and IV (black solid lines).

3.1. Overview of Uptake Experiments (Type A)

Two uptake chamber experiments are presented in Figure 1 showing the time courses of α-pinene, the total gas-phase HOMs, the organic aerosol (OA) mass concentration and the normalized OA for the two seed conditions Na_2SO_4 (Figure 1a) and $(NH_4)HSO_4$ (Figure 1b), respectively. Because the chamber was running in a CFR mode and aerosols were injected for 2 min only, OA mass concentration and seed were continuously diluted while the other parameters (HOMs, H_2O_2, α-pinene) were maintained in steady-state. To consider it, the organic mass concentration was normalized by the decrease of sulfate signal over the experiment time. The resulting normalized OA corresponds to the expected concentration without dilution effect and wall-loss, therefore also in a steady-state mode as all the other parameters (Figure 1). Details on the normalization protocol can be found in the corresponding Section S1 in Supporting Information S1.

Before the seed injection, rather constant total HOMs concentrations of about 6.5×10^8 and 5.9×10^8 molecules cm^{-3} were measured for the Na_2SO_4 and $(NH_4)HSO_4$ seed experiments, respectively. It is noteworthy that the total gas-phase concentrations given have to be considered as lower limits for the respective HOMs. The sensitivity of the HOMs detection via NO_3^--CI-APi-TOF-MS depends strongly on the chemical agent used for the ionization in combination with the functionalities of the HOMs. In the past, ionization with nitrate ions was the most commonly used (Bianchi et al., 2019; Ehn et al., 2014; Mutzel et al., 2015). For the lack of better standards, in situ produced H_2SO_4 was used as the calibration standard, which is expected to form more stable nitrate clusters than most HOMs. In more recent studies, however, other reagent ions such as acetate ions were found to be more sensitive toward HOM RO_2 with only one hydroperoxide group, resulting in higher yield estimates of up to a factor of three higher compared to ionization with nitrate (Berndt et al., 2016, 2015). Berndt et al. (2016) have shown that HOM yields from OH-radical induced oxidation of α-pinene have been significantly underestimated when using nitrate for ionization.

After seed injection, the total HOMs concentrations dropped by about 57% or 3.7×10^8 molecules cm^{-3} under Na_2SO_4 conditions and 42% or 2.5×10^8 molecules cm^{-3} under $(NH_4)HSO_4$ conditions, respectively. Subsequently, a HOMs recovery process took place under both seed conditions until the end of the experiments. However, this recovery process showed a much faster HOMs recovery in the first 30 min. During this time, significant differences in the behavior of OA mass concentrations were observed, depending on the type of seed particles. Under $(NH_4)HSO_4$ seed conditions, a continuous OA formation was observed for 30 min and reached its maximum at 90 min. Under Na_2SO_4 seed conditions however, OA kept decreasing until the end of the experiment. After the quick HOMs recovery process of 30 min, the HOMs concentrations in both experiments slowly recovered to the initial concentration level within 180 min. Based on the different behaviors of HOMs and OA throughout the experiments, the uptake experiments for both seed conditions can be split into four periods (I–IV, see below) which are sequentially discussed in the following Sections 3.2–3.4.

Period I: Pre-stabilization period without seed particles (first 60 min)
Period II: Initial uptake period directly after seed injection (4 min)
Period III: Transition period (following 30 min)
Period IV: HOMs regeneration period (until the end of the experiments).

3.2. Formation and Identification of Gas-Phase HOMs in Period I

During the period I, steady states of the gas-phase α-pinene oxidation were reached prior to the seed injection in both experiments, leading to a constant HOMs concentration. All possible HOMs assigned with m/z as well as their formation mechanisms are proposed by a comprehensive collection of previous studies (Berndt et al., 2016; Bianchi et al., 2019; Ehn et al., 2014; Jokinen et al., 2014; Mentel et al., 2015; Rissanen et al., 2014). The mechanism scheme is given in Figure S8 in Supporting Information S1. It should be noted that, in the present study, no organonitrates are considered due to the low background NO concentration that was below the detection limit of 100 ppt, as experiments were performed without any NO addition. To ensure a constant formation of closed-shell products, a comparatively high amount of H_2O_2 was introduced to the chamber. The mixing ratio can be estimated to be around 5 ppm based on the concentration of H_2O_2 in the gas saturator. This results in a high steady-state concentration of HO_2 radicals and thus, an increase of relative concentration of closed-shell products. Consequently, only HOM products with a fraction larger than 0.5% to the total HOMs are considered. Given this, all gas-phase HOM dimers are ignored due to their low fractions. In total, the resulting HOM products ($n = 39$) account for 78.0% and 77.5% of the total gas-phase HOMs formed under Na_2SO_4 and $(NH_4)HSO_4$ conditions, respectively. All concerned HOMs are listed in Table 1 and their corresponding time courses are given in Table S2 in Supporting Information S1. For each detected m/z signal, there are different possibilities for their chemical structure, since the HOMs identification has rarely been done on the molecular structure level. Therefore, formulas proposed in Table 1 are derived based on the summarized mechanism from literature shown in Figure S8 in Supporting Information S1. Nonetheless, the elementary formula of C10 HOMs can be quite reliable, since the formation of C11 and C9 products is barely possible from the OH-oxidation of α-pinene according to the known mechanism. These C10 HOMs are the dominant species measured in the present study (Table 1). In total, regarding the fractions of HOMs with respect to different C contents, the C10 HOMs account for 47.1% and 48.3%, while smaller molecular HOMs (i.e., C7 HOMs) account for 30.0% and 27.7% of total gas-phase HOMs under Na_2SO_4 and $(NH_4)HSO_4$ conditions, respectively. A closer look at the O/C ratios shows that smaller C7 HOMs (averaged O/C ratio of 0.82) are more oxygenated compared to C10 HOMs (averaged O/C ratio of 0.71).

3.3. Initial Uptake of HOMs During Period II

3.3.1. Determination of Uptake Coefficients

After the seed injection, aerosol particles can act as additional sink leading to reduced concentrations of HOMs as their vapor pressures are mostly low enough. Sink estimations given in Figure S6 in Supporting Information S1 illustrate that under the chosen steady-state flow reactor conditions, the particle condensation loss represents the dominant sink term for HOMs compared to other losses enabling the determination of uptake coefficients. A closer look into the first 4 min after seed injection (see period II in Figure 1) shows that the total HOMs concentrations dropped by about 57% or 3.7×10^8 molecules cm^{-3} under Na_2SO_4 conditions and 42% or 2.5×10^8 molecules cm^{-3} under $(NH_4)HSO_4$ conditions, respectively. The observed relative drops agree well with former

Table 1
Experimentally Determined Initial Uptake Coefficient (γ), Measured Mass, Molar Mass (MW), Proposed Formula, Corresponding O/C Ratio, Compound Class (CC, Defined in Section 3.4.1), and Contribution to the Total HOMs (f)

Measured mass	MW	Proposed formula	O/C	$\gamma(Na_2SO_4)$	$\gamma((NH_4)HSO_4)$	CC	*f*
208	146	$C_7H_{14}O_3$	0.43	$(2.7 \pm 0.3)\times10^{-2}$	NA[a]	A	7.8% (7.5%)
324	262	$C_{10}H_{14}O_8$	0.80	$(1.0 \pm 0.1)\times10^{-1}$	$(9.7 \pm 1.3)\times10^{-2}$	D	7.0% (7.6%)
310	248	$C_{10}H_{16}O_7$	0.70	$(1.2 \pm 0.1)\times10^{-1}$	$(7.7 \pm 0.9)\times10^{-2}$	C	5.4% (6.0%)
294	232	$C_{10}H_{16}O_6$	0.60	$(2.9 \pm 0.3)\times10^{-1}$	$(7.1 \pm 0.9)\times10^{-2}$	C	4.5% (4.5%)
312	250	$C_{10}H_{18}O_7$	0.70	$(1.2 \pm 0.1)\times10^{-1}$	$(9.7 \pm 1.1)\times10^{-2}$	C	3.7% (4.0%)
296	234	$C_{10}H_{18}O_6$	0.60	$(1.1 \pm 0.1)\times10^{-2}$	$(8.6 \pm 1.2)\times10^{-2}$	C	3.7% (4.0%)
220	158	$C_7H_{10}O_4$	0.57	$(3.1 \pm 0.4)\times10^{-2}$	NA	A	2.9% (2.4%)
278	216	$C_{10}H_{16}O_5$	0.50	$(7.2 \pm 0.9)\times10^{-2}$	$(3.6 \pm 0.4)\times10^{-2}$	B	2.9% (2.3%)
234	172	$C_7H_8O_5$	0.71	$(7.0 \pm 0.8)\times10^{-2}$	NA	A	2.7% (2.1%)
250	188	$C_7H_8O_6$	0.86	$(6.3 \pm 0.8)\times10^{-2}$	NA	A	2.5% (2.1%)
326	264	$C_{10}H_{16}O_8$	0.80	$(1.2 \pm 0.1)\times10^{-1}$	$(9.7 \pm 1.2)\times10^{-2}$	C	1.9% (2.0%)
341	279	$C_{10}H_{15}O_9$[b]	0.90	$(9.4 \pm 0.1)\times10^{-2}$	$(5.6 \pm 0.8)\times10^{-2}$	R	1.8% (1.9%)
308	246	$C_{10}H_{14}O_7$	0.70	$(1.0 \pm 0.3)\times10^{-1}$	$(4.8 \pm 0.6)\times10^{-2}$	D	1.8% (1.7%)
309	247	$C_{10}H_{15}O_7$[b]	0.70	$(7.2 \pm 0.1)\times10^{-2}$	$(4.9 \pm 0.6)\times10^{-2}$	R	1.6% (1.6%)
282	220	$C_7H_8O_8$	1.14	$(8.9 \pm 0.1)\times10^{-2}$	$(7.2 \pm 0.9)\times10^{-2}$	C	1.5% (1.5%)
325	263	$C_{10}H_{15}O_8$[b]	0.80	$(6.8 \pm 0.3)\times10^{-2}$	$(5.3 \pm 0.8)\times10^{-2}$	R	1.5% (1.5%)
238	176	$C_7H_{12}O_5$	0.71	$(5.4 \pm 0.1)\times10^{-2}$	$(2.3 \pm 0.3)\times10^{-2}$	B	1.5% (1.4%)
224	162	$C_7H_{14}O_4$	0.57	$(4.4 \pm 0.5)\times10^{-2}$	NA	A	1.4% (1.4%)
268	206	$C_7H_{10}O_7$	1.00	$(9.9 \pm 0.5)\times10^{-2}$	$(6.4 \pm 0.4)\times10^{-2}$	C	1.4% (1.3%)
280	218	$C_{10}H_{18}O_5$	0.50	$(8.6 \pm 1.2)\times10^{-2}$	$(7.3 \pm 0.7)\times10^{-2}$	B	1.4% (1.3%)
236	174	$C_7H_{10}O_5$	0.71	$(4.3 \pm 1.0)\times10^{-2}$	$(2.9 \pm 1.0)\times10^{-2}$	B	1.4% (1.3%)
342	280	$C_{10}H_{16}O_9$	0.90	$(1.1 \pm 0.8)\times10^{-1}$	$(8.6 \pm 0.5)\times10^{-2}$	D	1.2% (1.2%)
311	249	$C_{10}H_{17}O_7$[b]	0.70	$(5.9 \pm 0.1)\times10^{-2}$	$(3.8 \pm 0.6)\times10^{-2}$	R	1.2% (1.2%)
339	277	$C_{10}H_{13}O_9$[b]	0.90	$(1.0 \pm 0.1)\times10^{-1}$	$(5.3 \pm 1.4)\times10^{-2}$	R	1.2% (1.2%)
240	178	$C_7H_{14}O_5$	0.71	$(8.0 \pm 1.0)\times10^{-2}$	$(2.7 \pm 0.4)\times10^{-2}$	B	1.1% (1.2%)
340	278	$C_{10}H_{14}O_9$	0.90	$(1.4 \pm 0.2)\times10^{-1}$	$(9.9 \pm 1.2)\times10^{-2}$	D	1.1% (1.2%)
264	202	$C_{10}H_{18}O_4$	0.40	$(6.4 \pm 0.8)\times10^{-2}$	$(3.8 \pm 0.5)\times10^{-2}$	B	1.1% (1.1%)
252	190	$C_7H_{10}O_6$	0.86	$(7.0 \pm 0.9)\times10^{-2}$	$(4.7 \pm 0.5)\times10^{-2}$	B	1.1% (1.0%)
266	204	$C_7H_8O_7$	1.00	$(6.0 \pm 0.8)\times10^{-2}$	$(3.7 \pm 0.5)\times10^{-2}$	B	1.0% (1.0%)
276	214	$C_{10}H_{14}O_5$	0.50	$(5.6 \pm 0.8)\times10^{-2}$	$(4.7 \pm 0.5)\times10^{-2}$	X[c]	1.0% (1.0%)
292	230	$C_{10}H_{14}O_6$	0.60	$(8.8 \pm 1.1)\times10^{-2}$	$(4.7 \pm 0.5)\times10^{-2}$	X	1.0% (0.9%)
298	236	$C_7H_8O_9$	1.30	$(1.0 \pm 0.1)\times10^{-1}$	$(6.9 \pm 0.9)\times10^{-2}$	D	1.0% (0.9%)
262	200	$C_{10}H_{16}O_4$	0.40	$(6.5 \pm 0.9)\times10^{-2}$	$(3.7 \pm 0.4)\times10^{-2}$	B	0.8% (0.8%)
271	209	$C_7H_{13}O_7$[b]	1.00	$(3.3 \pm 0.5)\times10^{-2}$	NA	R	0.8% (0.7%)
357	295	$C_{10}H_{15}O_{10}$[b]	1.00	$(9.0 \pm 0.6)\times10^{-2}$	$(5.7 \pm 0.2)\times10^{-2}$	R	0.7% (0.7%)
297	235	$C_7H_7O_9$[b]	1.30	$(8.0 \pm 1.2)\times10^{-2}$	$(2.1 \pm 0.3)\times10^{-2}$	R	0.7% (0.7%)
222	160	$C_7H_{12}O_4$	0.57	$(4.2 \pm 1.2)\times10^{-2}$	$(1.6 \pm 0.7)\times10^{-2}$	B	0.7% (0.7%)
375	313	$C_{10}H_{17}O_{11}$[b]	1.10	$(1.4 \pm 0.2)\times10^{-1}$	$(8.8 \pm 1.2)\times10^{-2}$	R	0.6% (0.6%)
218	156	$C_7H_8O_4$	0.57	$(3.2 \pm 0.4)\times10^{-2}$	$(1.1 \pm 0.2)\times10^{-2}$	B	0.5% (0.5%)
Sum							78.0% (77.5%)

Note. f values obtained under (NH4)HSO4 seed conditions are given in the parentheses.
[a]NA, not available. [b]Rradicals. [c]Class X: others.

chamber experiments by Peräkylä et al. (2020). In their α-pinene oxidation experiments, they observed reductions by about 60% after seed injection.

Based on the individual drop of the gas-phase HOMs concentrations during this period II in Table S2 in Supporting Information S1, initial uptake coefficients γ for each detected single HOM compound have been calculated using the following equations (Ammann et al., 2013):

$$\frac{d[X]_g}{dt} = -k_{1st}[X]_g = -\gamma\frac{\overline{c}}{4}\mathrm{SSA}[X]_g \quad (1)$$

$$\gamma = -\frac{4}{\overline{c}\,\mathrm{SSA}\,[X]_g}\frac{d[X]_g}{dt} = \frac{4\,k_{1\mathrm{st}}}{\overline{c}\,\mathrm{SSA}} \quad (2)$$

$$\overline{c} = \sqrt{\frac{8RT}{\pi M}} \quad (3)$$

with the concentration $[X]_g$ of compound X in the gas phase in molecules cm^{-3}, the mean thermal velocity $\overline{c}$ (see Equation 3) of compound X in m s^{-1}, the universal gas constant R (8.31451 J K^{-1} mol^{-1}), the temperature T in K, the molar mass M of compound X in g mol^{-1}, the specific surface area (SSA; $\mathrm{SSA}_{\mathrm{Na2SO4}} = 1.30 \times 10^{-3}$ cm^{-1}; $\mathrm{SSA}_{\mathrm{(NH4)HSO4}} = 1.77 \times 10^{-3}$ cm^{-1}) of the seed particles in cm^{-1}, and the first-order rate loss coefficient k_{1st} of compound X. The latter has a dimension of s^{-1} and describes the concentration loss of a HOM compound in the gas phase due to particle uptake during period II. To calculate the uptake coefficient γ of a HOMs compound, the slope of the concentration decreases after the seed injection ($d[\mathrm{X}]_g/dt$) has been determined from the measured NO_3^--CI-APi-TOF-MS data. The slope values represent the minimum (maximum negative) slope of a 2 min moving data set during the 4 min period II. By rearranging Equation 1, both the uptake coefficient γ and the first-order rate loss coefficient k_{1st} of compound X can be calculated. For the sake of clarity, the calculation procedure is displayed in Figure S5 in Supporting Information S1. All calculated values are given in Table 1 and Table S2 in Supporting Information S1, respectively. It should be mentioned that district concentration drops, that is, noticeable changes from the pre-seed steady-state conditions, were also observed for RO_2-HOM compounds (see Table S2 in Supporting Information S1). This allowed for the determination of uptake coefficients γ also for RO_2 radicals which are reported in Table 1 and Table S2 in Supporting Information S1, too.

The first-order rate loss coefficients k_{1st} for the different HOMs under Na_2SO_4 and $(NH_4)HSO_4$ seed conditions (named k_{Na2SO4} and $k_{NH4HSO4}$ in Table S2 in Supporting Information S1) are in the range of 1.9×10^{-3}–7.0×10^{-3} s^{-1} and 0.9×10^{-3}–6.8×10^{-3} s^{-1}, respectively. The k_{1st} values under Na_2SO_4 seed conditions are on average a factor of 1.3 higher compared to the $(NH_4)HSO_4$ seed values implying an aerosol phase-state effect. In comparison to the low RH chamber experiments by Peräkylä et al. (2020), the NH_4HSO_4 seed k_{1st} value of $C_{10}H_{16}O_7$ ($m/z = 310$) is about times 2 lower in the present study. Considering the different measurement and calculation methods as well as chambers used in the two studies, a factor of 2 implies comparable values.

The initial uptake coefficients γ of all single HOM compounds are in the range of 1×10^{-2}–2×10^{-1} (see Table 1). These data are not affected by absolute sensitivity issues of the HOMs detection as they are discussed in Section S1 in Supporting Information S1, as relative changes are used for the determination of the uptake coefficients. Experimentally determined uptake coefficients from the present study have been found comparable to uptake coefficients measured for the uptake of the reactive compounds such as isoprene oxide IEPOX and α-pinene oxide to SOA particles (Drozd et al., 2013; Gaston et al., 2014; Lal et al., 2012).

Moreover, the results obtained in the present study show that γ values of HOMs taken up to Na_2SO_4 seed particles are on average 1.7 times higher than those to $(NH_4)HSO_4$ acidic seed particles. This can be attributed to the lower SSA of the Na_2SO_4 seed particles ($\mathrm{SSA}_{\mathrm{Na2SO4}}/\mathrm{SSA}_{\mathrm{(NH4)HSO4}} = 1.30 \times 10^{-3}/1.77 \times 10^{-3} = 0.73$), and the higher k_{1st} of HOMs decrease under Na_2SO_4 conditions (averaged $k_{1st\_Na2SO4}/k_{1st\_(NH4)HSO4} = 1.4$). According to Equation 2, the obtained difference between the γ values of the $(NH_4)HSO_4$ and the Na_2SO_4 seed can explained by these two factors. The difference in the k_{1st} (see Table S2 in Supporting Information S1) can be due to the different phase-states of the two seeds which can also cause differences in the initial uptake. Higher k_{1st} of HOMs for effloresced $(NH_4)HSO_4$ seed at low and for deliquesced $(NH_4)HSO_4$ seed at high RH conditions were found by Peräkylä et al. (2020) which suggests a seed state effect for the initial uptake.

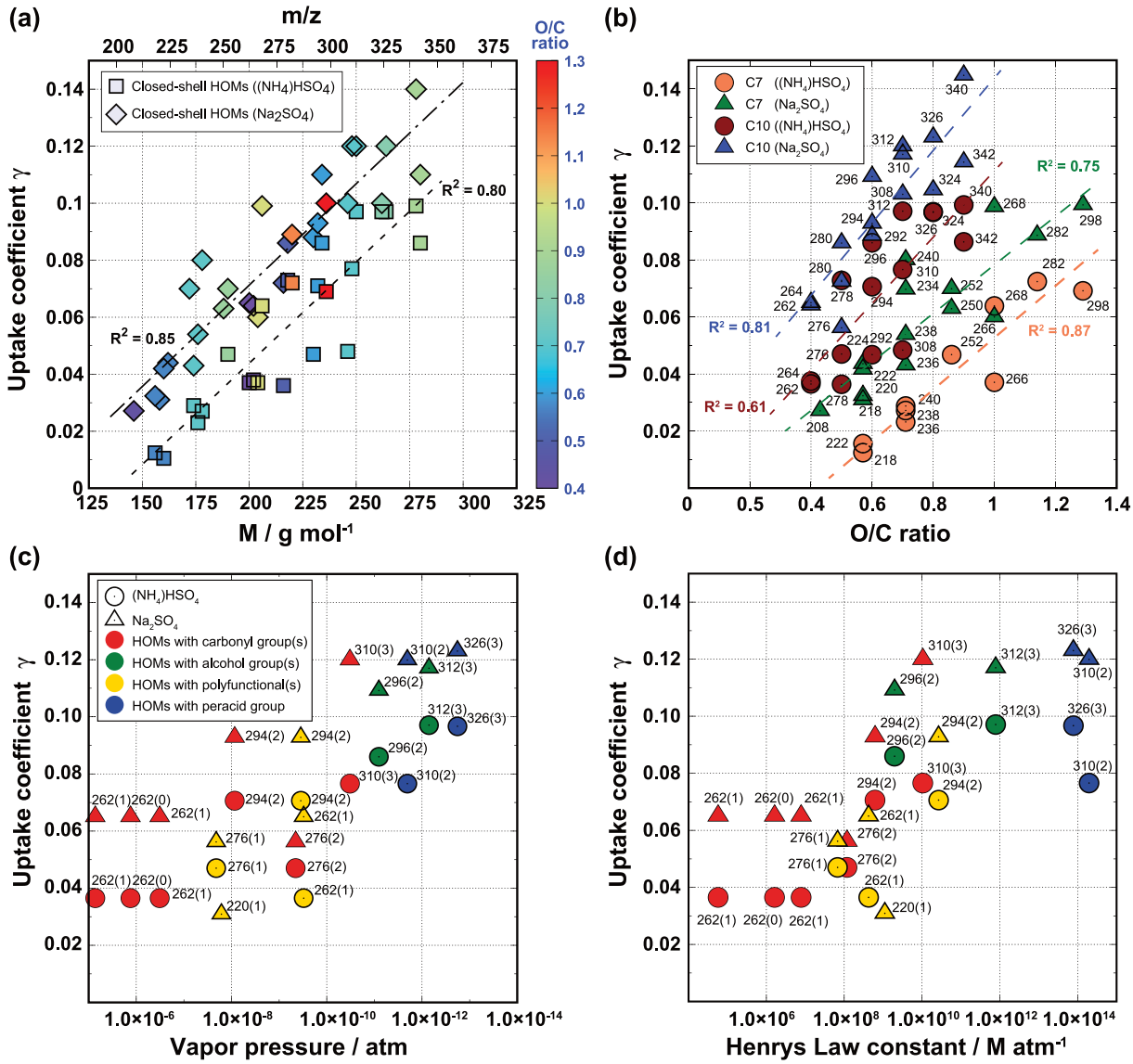

Figure 2. The calculated γ value for gas-particle uptake of highly oxygenated organic molecules (HOMs) as the functions of (a) molar mass, (b) O/C ratio, (c) vapor pressure and (d) Henry's law constant. Data points are sorted according to seed with Na_2SO_4 and $(NH_4)HSO_4$ seed marked by triangles/diamonds and circles/squares, respectively. Numbers in parenthesis indicate the number of ROOR/ROOH groups in a molecule.

3.3.2. Relationships Between the Measured HOMs Uptake Coefficients and Their Chemical Structures/ Physicochemical Properties

To examine the difference in the uptake behaviors among individual HOM compounds in more detail, relationships between uptake coefficients and chemical structural information of the investigated HOMs were analyzed. First, the calculated γ values of each closed-shell HOMs were compared to their respective molar mass (Figure 2a; similar plot for the RO_2-HOMs given in Figure S9 in Supporting Information S1), and the oxygen-carbon (O/C) ratio based on a defined chemical structure (Figure 2b) for the two different aerosol seeds. For both seeds, the uptake coefficient of the closed-shell HOMs increased together with their molar mass (Figure 2a), however, with slightly higher γ values for the Na_2SO_4 seed compared to $(NH_4)HSO_4$. A similar observation is made when comparing the γ values of the radicals for the two types of seeds (Table 1). Furthermore, the uptake coefficients of the closed-shell HOMs products are higher compared to detected radical products (see Figure S9 in Supporting Information S1). Looking at the corresponding O/C ratio of each of the closed-shell HOMs, it is not possible to link it to the change in the γ values since the O/C values are randomly distributed (Figure 2a). However, a

quite different conclusion can be drawn when looking at a specific number of carbon atoms like C7 and C10 (Figure 2b). In this case, a clear increase in the γ values with an increasing O/C ratio can be reported, indicating a stronger uptake of more oxidized HOMs in agreement with previous works (e.g., Peräkylä et al., 2020). This dependency is increasing with a higher number of carbon atoms in the HOM molecules, shown by a steeper slope for C_{10}- than for C_7-HOMs. As reported for the molecular mass correlation, the type of the seeds seems to also influence dependency between the O/C ratio and the γ values (initial uptake), with a higher slope for the Na_2SO_4 seed. These results indicate that the potential contribution of the C10 HOMs to the SOA formation is higher than that of the C7 compounds.

The good correlation between the molar mass and gamma observed here agrees with the results of Peräkylä et al. (2020) for HOMs from α-pinene ozonolysis experiments. These authors investigated the fraction of HOMs remaining after seed injection as a function of the mass of the detected cluster. They found that for clusters with lower cluster masses ($M + NO_3^-$ ion <250 Da) almost no uptake occurs. For HOM monomers with masses >350 Da ($M + NO_3^-$ ion), they observed gas-phase reductions of about 70% but no further decrease for HOMs with even higher molecular mass. A sigmoidal transition was observed between the two extremes, associated with a gradual decrease of volatility with increasing mass. The finding of the present study of a stronger uptake for compounds with higher molecular mass is consistent with the results of Peräkylä et al. (2020). However, in the present study, we have only focused on HOM monomers ($M + NO_3^-$ ion <375 Da). The gradual increase and good linear correlation are related to this fact.

The dependencies of the γ values on the functional groups associated with the individual HOMs and their related physicochemical properties (vapor pressure and Henry's law constant) were further investigated to identify potential relationships. However, it should be noted that these investigations have used these two parameters only as potential proxy for other key physicochemical HOM properties such as polarity, etc. It is not assumed that the two applied seed particles at these very low RH conditions consist exclusively in an aqueous- or liquid-phase state but small amounts of condensed-phase water can be associated with the particle surface (see Section 2.3).

Vapor pressures and the Henry's law constants for each of the closed-shell HOMs products were calculated by EVAPORATION (Compernolle et al., 2011) using the UManSysProp v1.0 facility (Topping et al., 2016) and HENRYWIN (Meylan & Howard, 1991; US-EPA, 2012), respectively. However, these two approaches require knowledge about the chemical structures of each considered closed-shell HOM. Unfortunately, due to the rather coarse mass resolution of the cTOF that equipped our NO_3^--CI-APi-TOF-MS, different chemical compositions are possible for a single observed m/z ratio. Although, estimation results can be found for all the close-shell HOM compounds (Figure S8 in Supporting Information S1), only selected HOMs data, which have been proposed from previous studies, are considered in Figures 2c and 2d.

Figure 2c depicts the calculated vapor pressures as the function of the observed uptake coefficients for both the Na_2SO_4 and $(NH_4)HSO_4$ seeds. The calculated vapor pressures cover eight orders of magnitude range from 10^{-13} to 10^{-5} atm. It can be seen that the vapor pressures of HOMs carrying no or only one ROOR/ROOH functionality are lower than HOMs having more ROOR/ROOH moieties or even a peracid functionality. Accordingly, Figure 2c shows higher γ values with decreasing vapor pressures. However, the γ value increases not exclusively as a function of the vapor pressure, as similar γ values are observed for different HOMs which have orders of magnitude different vapor pressures. Similar to the variation of the predicted vapor pressures, the calculated Henry's law constants show a broad variation between the different HOMs with values ranging from 10^4 M atm^{-1} for HOMs with carbonyl groups to 10^{14} M atm^{-1} for HOMs with peracid groups. For HOMs with more ROOR/ROOH/R(O)OOH moieties, higher Henry's law constants and higher γ values can be observed.

Overall, good correlations ($R^2 = 0.80/0.85$ under $(NH_4)HSO_4/Na_2SO_4$ seed conditions) were found between the uptake coefficient and their molar mass, which might be useful for the development of a γ estimation method. Meanwhile, the results demonstrate a relationship between the HOMs uptake coefficients and their degree of functionalization. The numbers of ROOR/ROOH/RC(O)OOH functions resulting from the autoxidation processes can be linked to the measured uptake coefficients. Furthermore, the aerosol seed crucially affects the uptake coefficients of HOMs, as γ values are significantly higher under Na_2SO_4 seed conditions compared to those under $(NH_4)HSO_4$ seed conditions. Nevertheless, more precise identifications of HOMs on the molecular structure level are of great necessity to improve the understanding of the impact of physicochemical properties on HOMs uptake coefficients.

3.3.3. Estimated Contribution of HOMs to the OA in Experiment Period II

Gas-phase HOMs uptake and their subsequent reactions in the particle-phase lead to the particulate OA formation. During the decrease of the HOMs in period II, 0.82 and 1.98 μg m^{-3} OA were formed under Na_2SO_4 and $(NH_4)HSO_4$ seed conductions, respectively. The contribution of the HOMs to the total OA ($f_{HOMs/OA}(t) = [HOMs]_t/[OA]_t$) was compared to their uptake coefficient during period II (Figure S10 in Supporting Information S1) for the two different seed experiments.

Basically, increasing trends can be found for the possible contributions of single HOM compounds to OA formation with the increase of γ under both seed conditions. Meanwhile, not only the uptake coefficients, but also the $f_{HOMs/OA}$ of individual gas-phase HOMs are higher for the use of Na_2SO_4 seed particles. Summing up the $f_{HOMs/OA}$, the uptake of total HOMs on $(NH_4)HSO_4$ and Na_2SO_4 seed particles contribute 5.3% and 15.3% to the OA formation, respectively. This nearly three times higher $f_{HOMs/OA}$ under Na_2SO_4 seed conditions can be mainly attributed to less OA formation (2.4 times less OA for the use of Na_2SO_4 seeds compared to the use of $(NH_4)HSO_4$ ones) and the higher HOMs uptake. However, it should be noted that these yields have to be considered as lower limits, as it has been already demonstrated that operating NO_3^--APi-ToF-MS with other ionization techniques could enable for a detection of not only a wider range but also a high concentration of oxygenated volatile organic compounds (OVOCs; Bianchi et al., 2019). This might lead to a more comprehensive evaluation of atmospheric HOMs concentrations and consequently, to higher OA mass fraction.

3.3.4. Analysis of the Different Uptake Resistances

To clarify whether the experimentally determined total γ is limited by individual processes in the gas and/or the particle-phase, the resistance model by Schwartz was applied (Finlayson-Pitts & Pitts, 2000; Schwartz, 1986). According to the resistance model, the total uptake coefficient γ_{tot} is given by:

$$\frac{1}{\gamma_{tot}} = \frac{1}{\gamma_g} + \frac{1}{\alpha} + \frac{1}{\gamma_{sol} + \gamma_{rxn}} \tag{4}$$

with the specific uptake coefficients γ_g, γ_{sol}, and γ_{rxn} for diffusion in gas phase, solution, and reaction in a bulk phase, as well as the mass accommodation coefficient α. The specific uptake coefficients γ_g, γ_{sol} and γ_{rxn} can be estimated according to the following equations:

$$\gamma_g = \frac{8D_g}{\bar{c}\, d_{\text{particle}}} \tag{5}$$

$$\gamma_{sol} = \frac{8HRT\sqrt{D_b}}{\bar{c}\sqrt{\pi t}} \tag{6}$$

$$\gamma_{rxn} = \frac{4HRT\sqrt{kD_b}}{\bar{c}} \tag{7}$$

with gas-phase diffusion coefficient D_g in $m^2\ s^{-1}$, mean thermal velocity $\bar{c}$ in m s^{-1}, particle diameter d_{particle} in m, Henry's law constant H in M atm^{-1}, temperature T in K, gas constant R in atm L mol^{-1} K^{-1}, bulk phase diffusion coefficient D_b in $m^2\ s^{-1}$, exposure time t in s and first-order reaction rate constant k in s^{-1}. Further parameters used for estimation are given in Table S3 in Supporting Information S1.

In the resistance model, key parameters such as gas-phase diffusion coefficient (D_g), mass accommodation factor (α) and bulk-phase diffusion coefficient (D_b) have been varied. Selected results are shown in Figure 3. The investigations of the individual resistances showed that a variation of the gas-phase diffusion coefficient D_g in a reasonable range of (0.1–1) × 10^{-6} $m^2\ s^{-1}$ has almost no limiting effect on the uptake. Even if α becomes 1, which is close to the value of 0.88 for LVOC/SVOC to organic surface reported by Liu et al. (2019), $1/\gamma_g$ only adds to a minor fraction of 0.2–$1/\gamma_{tot}$ (Figure 3a). For further calculations, D_g was set to 5.5 × 10^{-6} $m^2\ s^{-1}$ as estimated for HOMs with an increment system (Fuller et al., 1966; Mennola et al., 2003). Likewise, the variation of the bulk-phase diffusion coefficient D_b in a dissimilar range of 1 × 10^{-10}–1 × 10^{-20} $m^2\ s^{-1}$ for a liquid to semi-solid particle-phase, only has a negligible limiting effect ($f(1/(\gamma_{sol} + \gamma_{rxn})) < 0.01$) on the uptake in the range of a semi-solid particle-phase ($D_b \sim 1 \times 10^{-20}$ $m^2\ s^{-1}$; Figure 3b). This is due to the high Henry's law constant H resulting in a small aerosol resistance term $1/(\gamma_{sol} + \gamma_{rxn})$ shown in Figure 3b for the fraction of $1/(\gamma_{sol} + \gamma_{rxn})$

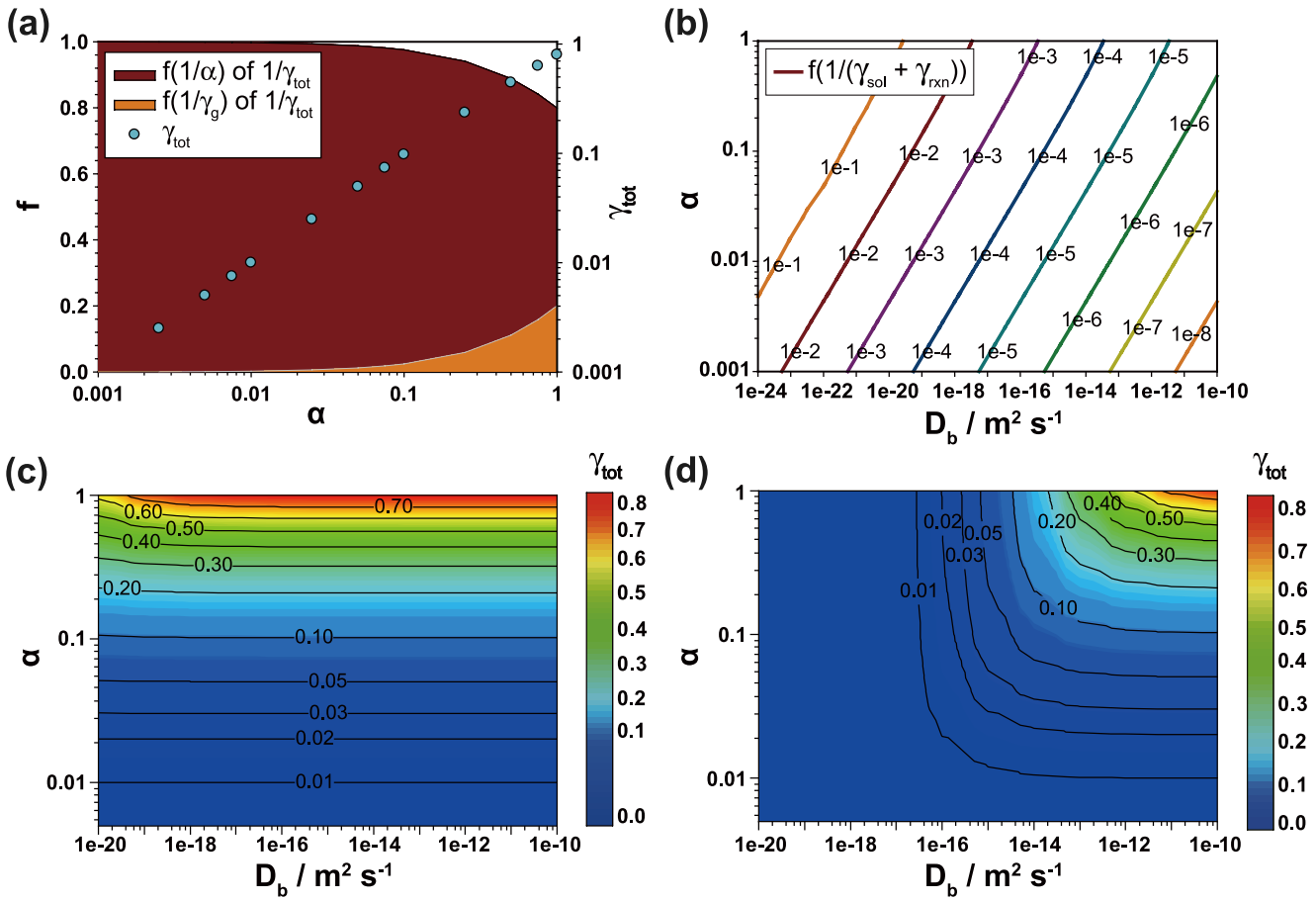

Figure 3. (a) Fractions of the resistance terms $1/\gamma_g$ and $1/\alpha$ of $1/\gamma_{tot}$, as well as γ_{tot} as a function of α for $C_{10}H_{18}O_7$; (b) fraction of $1/(\gamma_{sol} + \gamma_{rxn})$ of $1/\gamma_{tot}$ as a function of α and bulk-phase diffusion coefficient D_b for $C_{10}H_{18}O_7$; γ_{tot} as a function of α and bulk-phase diffusion coefficient D_b for selected HOMs $C_{10}H_{18}O_7$ (c) and $C_{10}H_{16}O_5$ (d).

of $1/\gamma_{tot}$. Over the whole range of D_b, the mass accommodation coefficient α is the major limiting factor for the uptake of HOM compounds with a high Henry's law constant H, such as $C_{10}H_{18}O_7$ (m/z 312 $[M + NO_3]^-$) for listed conditions (Figure 3c). In case of HOM products with a lower Henry's law constant H (i.e., $C_{10}H_{16}O_5$ (m/z 278 $[M + NO_3]^-$), the diffusion and reaction in bulk phase play a more decisive role under semi-solid particle-phase conditions (Figure 3d).

Overall, the uptake coefficients were obtained for each individual HOMs during period II under both Na_2SO_4 and $(NH_4)HSO_4$ seed conditions. In this period, stronger initial uptake behaviors were observed for the use of Na_2SO_4 particles, whereas more OA formation was found under $(NH_4)HSO_4$ seed conditions. In addition to the initial uptakes, different concentration patterns can be observed for individual HOMs under two seed conditions in the subsequent reactive uptake periods, which are to be discussed in the following section.

3.4. Reactive HOMs Uptake and OA Formation During Periods III and IV

Following the concentration drop in period II, the concentration of gas-phase HOMs recovered over the experimental time due to the flushing out and wall loss of the seed particles and therefore loss of surface for condensation, as well as the possible occurrence of HOMs saturation on the particle surfaces. This recovery proceeded in two periods called periods III and IV under both seed conditions (Figure 1). Period III corresponds to a fast return of the gas-phase HOMs concentration under both seed conditions, but with a continuous OA formation observed only under $(NH_4)HSO_4$ seed condition, while period IV is characterized by a rather slow recovery process until the total removal of particles from the chamber (see Figure 1 and MPSS data in Figure S4 in Supporting Information S1).

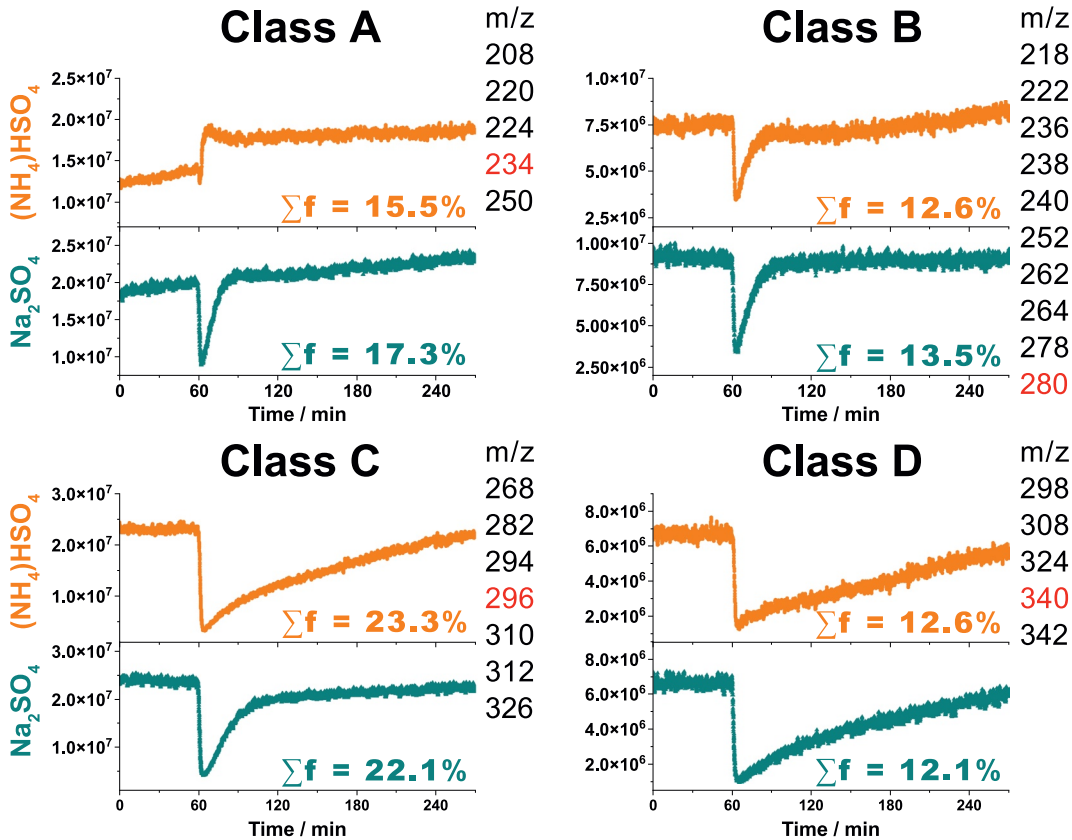

Figure 4. Classification of highly oxygenated organic molecules (HOMs) according to their typical time courses under both Na_2SO_4 and $(NH_4)HSO_4$ seed conditions. The *m/z* of the respective HOMs plotted are marked in red. The fraction of individual HOMs to total HOMs in each class are summed up according to Table 1 and given at the bottom-right corner in each subplot.

3.4.1. HOMs Classification Regarding Their Common Uptake Behaviors

A closer look into the time profiles of each individual HOM compounds in periods III and IV (Table S2 in Supporting Information S1) reveals the presence of several classes of uptake behaviors. Closed-shell HOMs were grouped in four classes named A, B, C, and D (see Figure 4 and Table 1), all characterized by even *m/z* ratios. In contrast to closed-shell HOMs, radical HOMs have odd *m/z* ratios and were grouped in class R. In general, the molar mass of HOMs in different classes is increasing from A to D, and their oxygen content follows the same trend.

Five HOMs are classified into class A and they are all identified as C7 HOMs corresponding to the smallest molecular compounds. In contrary to the other classes, Class A shows a distinct behavior for the two seeds (Figure 4). A rapid growth in the gas phase during period II and partly period III was observed with the $(NH_4)HSO_4$ seed for HOMs in class A, while the concentration decreased during period II for the Na_2SO_4 seed as observed for all other classes. The increase of gas-phase concentrations for class A HOMs upon seed injection of $(NH_4)HSO_4$ particles implies that some fragmentation reactions may occur in or on $(NH_4)HSO_4$ particles. As proposed by Mutzel et al. (2015) and observed by Peräkylä et al. (2020), heterogeneous fragmentation reactions can result in a degradation of larger HOMs to smaller carbonyl compounds that could then evaporate to the gas phase because of their higher vapor pressures and lead to an increase of the class A HOMs gas-phase concentration levels compared to the pre-seed period I. Class B includes HOMs showing regular uptake behaviors with only initial uptake under both seed conditions. The HOMs concentration in this class fully recovered to the initial level during period III and there are no obvious differences under both seed conditions. The recovery to the pre-seed concentration level is caused by the continuously decreasing condensation sink due to the dilution of the seed aerosol in the chamber through flush-out and wall losses of aerosols. For more oxygenated HOMs

in class C with larger *m*/*z* and oxygen contents of 6–7 (Table 1), a slower recovery to the pre-seed concentration level under acidic $(NH_4)HSO_4$ seed condition is observed suggesting an continuous reactive uptake occurring during period III and IV under acidic $(NH_4)HSO_4$ seed conditions. Perhaps, effective acidity-driven reactions in the particle-phase can consume more HOMs than are refilled by condensation from the gas phase leading to an undersaturation of these HOMs in the particle-phase. This undersaturation induces further uptake and a delayed return to the pre-seed concentration level under $(NH_4)HSO_4$ seed condition, a so-called reactive uptake behavior. When HOMs get extremely highly oxygenated (class D HOMs with the highest *m*/*z* and oxygen contents of 7–9), their concentration slowly returns to the pre-seed levels, suggesting a reactive uptake for both seed conditions which can be attributed to the presence of more hydroperoxyl groups in their chemical structures. Multiple mechanisms have been proposed for the degradation of hydroperoxides on atmospheric particles. The decompositions of α-hydroxy-hydroperoxides, as well as peroxyacetic acid has been reported to lead to the formation of hydrogen peroxide and aldehydes (O'Sullivan et al., 1996; Staffelbach & Kok, 1993; Zhou & Lee, 1992). Similarly, acid-catalyzed reactions lead to the formation of alcohols and smaller degradation products (Enami, 2021). Additionally, the comparatively weak O-O bond of hydroperoxyl groups is prone to homolytical cleavage by photolysis, forming alkoxy- and hydroxyl radicals. In this case, a continuous removal of hydroperoxyl HOMs cannot be ruled out, as experiments were performed under illumination (Chen et al., 2011; Krapf et al., 2016; Li et al., 2016; Pospisilova et al., 2021) and thus, condensational saturation of class D HOMs in the particle-phase can hardly be reached, resulting in the continuous reactive uptake of HOMs under both seed conditions. Similar to heterogenous reactions, photodegradation of HOMs after partitioning could result in the formation of smaller fragments as well as enhance particle-phase reactions (Pospisilova et al., 2021). As smaller HOMs with less carbon atoms might be much more volatile, such products might partition to the gas phase, which would explain the increase of gas-phase concentrations for class A HOMs for $(NH_4)HSO_4$ seed particles. In the case of Na_2SO_4 seed particles, the overall smaller fraction of OA might prevent the evaporation of such degradation products and/or their solid state suppress photolysis processes (Wong et al., 2015).

The γ values and $f_{HOMs/OA}$ of HOMs in each class can be found in Figure S11 in Supporting Information S1. The uptake coefficients of HOMs in classes A and B are obviously smaller than those in classes C and D. Considering the molar mass of HOMs in different classes, this is in line with our finding that uptake coefficients of HOMs are positively correlated to their molar masses. Meanwhile, similar relationships can be found for $f_{HOMs/OA}$ of individual HOM compounds. Summing up the $f_{HOMs/OA}$ of HOMs in each class, it can be seen that class C dominates the OA formation induced by HOMs condensation under both seed conditions (2.3% and 5.6% in Na_2SO_4 and $(NH_4)HSO_4$ seeds, respectively), and class D can also play a significant role (1.4% and 3.4% in Na_2SO_4 and $(NH_4)HSO_4$ seeds, respectively). Unsurprisingly, class C also represents a dominant HOMs fraction (Σf) contributing to 22.1% and 23.3% under Na_2SO_4 and $(NH_4)HSO_4$ seed conditions, respectively. Meanwhile, class B HOMs have a similar Σf than class D HOMs but a much lower $f_{HOMs/OA}$. This finding suggests that HOMs in Class B are less favorable in the uptake processes which is in line with their lower γ values (Figure S11 in Supporting Information S1). Likewise, Class A HOMs are the most unfavorable for condensation with the lowest γ values (Figure S11 in Supporting Information S1). To get a better understanding of the different behaviors of HOMs in different classes, further investigations on the identification of accurate chemical structures of these HOMs are encouraged.

3.4.2. Total OA Mass Formation

In period III, similar behaviors can be observed for the total HOMs under both seed conditions. About 65.5% (2.37×10^8 molecules cm^{-3}) and 64.8% (1.56×10^8 molecules cm^{-3}) of HOMs were regained under Na_2SO_4 and $(NH_4)HSO_4$ conditions, respectively (Figure 1). However, a significant difference in particle-phase OA formation was found during this period when comparing the two experiments using different types of seeds. Under acidic non-solid $(NH_4)HSO_4$ seed conditions, OA is slowly growing during period III, reaching the maximum concentration of 2.5 μg m^{-3} at the end of this period, whereas the OA mass concentration is continuously decreasing under the neutral solid Na_2SO_4 seed condition throughout periods III and IV (Figure 1). At the beginning of the period III, an organic coating thickness of about 2 nm for both seeds was estimated consisting of a few molecular layers of organic compounds around the seed particles. To exclude the chamber dilution effect, OA mass concentrations were normalized from the dilution ratio using the measured sulfate mass concentrations directly after injection as dilution factors (Figure 1 and method description in the SI). From the normalized OA mass concentration, OA formation rates of 52.9 and 22.4 ng m^{-3} min^{-1} (Figure 1) were calculated for $(NH_4)HSO_4$ and Na_2SO_4 seeds, respectively. This result clearly indicates the presence of a reactive uptake process of the HOMs,

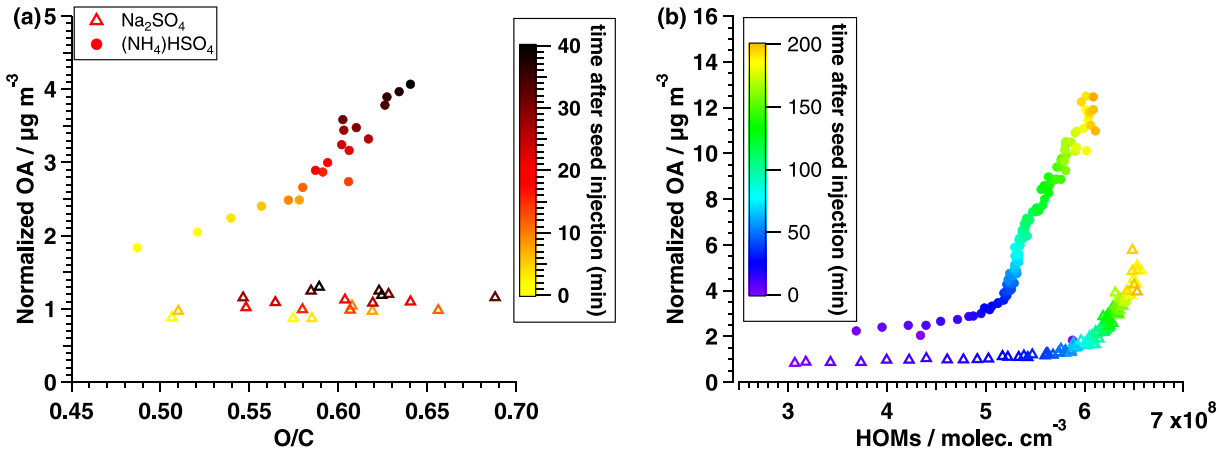

Figure 5. Normalized organic aerosol (OA) concentration as the functions of particle-phase O/C ratio (a) and total gas-phase highly oxygenated organic molecules (HOMs) concentration (b) under $(NH_4)HSO_4$ (circles) and Na_2SO_4 (triangles) seed conditions color-coded with the time after aerosol seed injection.

that is, continuously loss behavior, under both seed conditions. However, the more acidic surface conditions and/or the different phase-state of the $(NH_4)HSO_4$ seed may significantly enhance particulate OA formation as the growth rate for those seed particles is by a factor of three higher than for Na_2SO_4 ones. An enhanced SOA formation under dry chamber conditions was also observed by Riva et al. (2019) when using $(NH_4)HSO_4$ instead of $(NH_4)_2SO_4$ seed. However, using the same set of experiments, Peräkylä et al. (2020) have found just small differences in the pattern of the gas-phase oxidation products using $(NH_4)HSO_4$ and $(NH_4)_2SO_4$ seeds. Therefore, Peräkylä et al. (2020) concluded that the SOA difference was not caused by enhanced HOM uptake. However, in the present study, differences in the uptake behavior of HOMs were detected perhaps of the use of Na_2SO_4 seed which is much more chemically inert than $(NH_4)_2SO_4$. It is important to note that due to the difference on the seed particles states (solid for Na_2SO_4 and non-solid for $(NH_4)HSO_4$), a small contribution of it on the partitioning cannot be completely excluded.

Furthermore, Figure 5 confirms the acidity-driven reactions of HOMs in particle-phase. Under acidic non-solid $(NH_4)HSO_4$ seed conditions, the temporal increase of the normalized OA mass concentration can be associated with the temporal increase of the O/C ratio of particles (Figure 5a), which supports an occurring particle-phase reaction process leading to the formation of more highly oxygenated compounds. The HOMs saturation in acidic $(NH_4)HSO_4$ seed particles were therefore reduced, and continuous condensation is enabled. A similar dependency can hardly be found for Na_2SO_4 seed particles. Figure 5a shows neither a temporal increase of the normalized OA nor a clear temporal trend in the O/C ratio for Na_2SO_4 seed conditions as well as no link between both parameters. This is supported when comparing the Class A HOMs with the measured OA mass concentration (Figure S12 in Supporting Information S1), where this type of HOMs show an increase of their gas-phase concentration after seed injection, presenting a close behavior than the OA mass concentration for the $(NH_4)HSO_4$ seed, while the same HOMs presents a typical uptake profile for the Na_2SO_4 seed conditions.

Figure 5b presents the normalized OA mass concentration against the total HOMs concentration as the function of the time after the seed aerosol injection. Under Na_2SO_4 seed conditions, an increase of the normalized OA mass concentration was found in period IV (after 90 min, i.e., when the gas-particle equilibrium was regained for most HOMs). This is in line with our initial hypothesis that mainly the initial uptake contributes to the OA formation under dry Na_2SO_4 seed condition. Only after a certain time when certain amount of organic matter has formed on the solid Na_2SO_4 seed, an increased OA formation can occur resulting in a delayed increase of the normalized OA compared to the expected non-solid $(NH_4)HSO_4$ seed. In contrary, for the $(NH_4)HSO_4$ seed condition, an almost linear relationship was observed between the normalized OA mass concentration and the total gas-phase HOMs concentration during period IV (90–200 min), which further supports the continuously reactive uptake process after the initial uptake. As higher seed acidity together with the expected non-solid aerosol phase state are driving the reactive uptake mechanism, acid-catalyzed reactions may be the predominant sinks of HOMs under $(NH_4)HSO_4$ seed conditions. Such acid-catalyzed reactions are already well-known for compounds such as IEPOX and was further observed for smaller hydroperoxides (Gaston et al., 2014; Nguyen et al., 2014;

Riva et al., 2017; Tilgner et al., 2021). Possible mechanisms for acid-catalyzed reactions are ring opening of epoxide structures, known for epoxides from isoprene oxidation, but also intramolecular rearrangement reactions (D'Ambro et al., 2017; Mutzel et al., 2015; Surratt et al., 2010). Since different behaviors of HOMs uptake were observed under the Na_2SO_4 and $(NH_4)HSO_4$ seeds conditions, it is of great necessity to focus on the identification of the particulate chemical composition in order to see the differences on the detected particle-phase species under different seed conditions. Although the type of the seed is clearly affected the partitioning of the HOMs, we cannot exclude similar behavior for the other oxidation products of the α-pinene that might also affect the overall OA mass concentration cannot be also completely excluded.

3.5. Identification of Particulate HOMs and Their Reaction Products by Filter Experiments (B)

To further identify the particulate organic compounds formed and to further understand the uptake and chemical processing, filter-based particle-phase analysis was performed regarding the detection of HOMs, organosulfates including HOOS, small carbonyl compounds and typical SOA markers from α-pinene OH oxidation using the experiment type B. All organic compounds detected in the particle-phase are listed in Table S4 in Supporting Information S1. Some of the detected m/z can be assigned to known SOA marker compounds from α-pinene oxidation, for example, m/z 199 and 187 to hydroxy-pinonic acid and hydroxy-terpenylic acid, respectively. These marker compounds are known products from secondary chemistry, mainly oxidation of pinonaldehyde and myrtenal (Mutzel et al., 2016), indicating the presence of both HOMs-related and also other, more classical SOA formation mechanisms. Possible mechanisms for their formation were discussed earlier for α-pinene ozonolysis by Mutzel et al. (2015). No dimers HOMs were detected in the filter experiments (B) of this study, which is in accordance with the measured HOMs results in the gas phase from the uptake experiments (A). Additionally, dimers have been shown to evade detection in filter analysis as previously reported by X. Zhang et al. (2017).

Looking closely at the particulate organic compounds produced from α-pinene/OH oxidation, six HOMs were detected offline on the particulate phase and are listed in the first section of Table S4 in Supporting Information S1. All these HOMs have also been observed in the uptake experiments, and their suggested HOMs structure from gas phase has been assigned. These six HOMs belong to either class B ($C_{10}H_{16}O_4$, $C_{10}H_{16}O_5$, and $C_{10}H_{18}O_5$) or class C ($C_{10}H_{18}O_6$, $C_{10}H_{18}O_7$, and $C_{10}H_{16}O_6$). Differences can be observed between these two classes: all off-line HOMs were observed predominantly in Na_2SO_4 seed particles, while no class C HOMs were detected in acidic $(NH_4)HSO_4$ seed particles. The absence of the most oxygenated HOMs (class C) in acidic $(NH_4)HSO_4$ seed particles further supports our hypothesis that these HOMs undergo acidity-driven reactions in the particle-phase, leading to an missing saturation, continuous uptake and increased OA formation.

The detection of one compound ($C_{10}H_{16}O_5$) after derivatization with 2,4-dinitrophenylhydrazone indicates the existence of a carbonyl moiety under both seed conditions. As already known, acidity has led to the formation of organosulfates and hints at a highly reactive environment in the particle-phase. But possible surface chemistry processes at higher pH values might also promote the decay of hydroperoxides as discussed before. With half-live times of 3–60 min, it has to be assumed that partitioned HOMs are not stable and might not be detected in their original structure (Krapf et al., 2016; Zhou & Lee, 1992). The identification of diaterebic acid acetate (DTAA) supports this view. Additionally, several compounds with lower oxygen content (C10H16O2-4) were detected and listed in the second section of Table S4 in Supporting Information S1. The presence of these compounds can be explained by both (a) gas-phase formation and subsequent partitioning and (b) by known decomposition reactions of C10 HOMs accompanied by loss of oxygen, including mechanisms with homolytic and acid-catalyzed O-O bond breakage with subsequent C-C bond breakage, but also rearrangement reactions maintaining the carbon chain (Cooper, 1951; Hock & Lang, 1944; R. Zhao, Lee, et al., 2013). Noteworthily, consecutive reactions with OH radicals and/or H_2O_2 as well as photolysis (Pospisilova et al., 2021; Wong et al., 2015) can again oxidize the condensed HOMs and their oxidation products, leading to the formation of compounds with the same chemical sum formula as that of detected gas-phase HOMs but different structures (von Sonntag & Schuchmann, 1991; R. Zhao, Lee, et al., 2013).

Apart from the C_{10} compounds, compounds with 7–9 carbon atoms were found in the particulate phase. Most of them were detected for both seeds, although in lower amounts in the $(NH_4)HSO_4$ seed regime (see chromatograms in Figure S13 in Supporting Information S1). In addition, small carbonyl compounds like glyoxal and glyoxylic acid are present in both seeds, indicating particle-phase reactions as a source of the $C_7 - C_9$ compounds. Particle-phase decomposition reactions of C_{10} compounds would result in the formation of $C_7 - C_9$ in combination

with $C_1 - C_3$ compounds. Based on the summarized mechanism in Figure S8 in Supporting Information S1, only C_7 HOMs formations are proposed in the gas phase, and thus condensation can be considered as another source of C_7 compounds.

Moreover, it has been shown that the condensation and chemical condensed-phase reactions of HOMs from α-pinene ozonolysis leads to the formation of HOOS (Brüggemann et al., 2017; Mutzel et al., 2015). In the present study, a similar process was observed for the uptake of HOMs from α-pinene/OH oxidation under $(NH_4)HSO_4$ seed conditions. The acid-enhanced formation of particle-phase OA leading to the formation of organosulfate compounds is supported by both the identification of the sulfur-containing organic fragments from AMS measurements (CH_3SO_2 and C_4HSO, Figure S14 in Supporting Information S1) and the identification of C_7 and C_{10} organosulfates from the filter measurements for acidic $(NH_4)HSO_4$ seed only (Table S4 in Supporting Information S1). As listed in Table S4 in Supporting Information S1, eight C_7 and C_{10} organosulfates were detected only under acidic $(NH_4)HSO_4$ seed conditions. Four of those (m/z 239, 249, 279, and 281, $[M–H]^-$) were observed before in the field as well as in laboratory-generated aerosol particles (Brüggemann et al., 2017, 2020; Mutzel et al., 2015; Surratt et al., 2007, 2008). Mechanistically, the formation of organosulfate compounds under $(NH_4)HSO_4$ seed conditions can be explained to occur after initial decomposition of HOMs at their hydroperoxide groups, for example, through the Korcek mechanism, followed by the nucleophilic attack of HSO_4^- and/or electrophilic addition, and a subsequent loss of O_2, HO_2 or OH (Brüggemann et al., 2017, 2020; Iinuma et al., 2009; Minerath & Elrod, 2009; Riva et al., 2016; Surratt et al., 2007). Such a reaction mechanism further supports the absence of hydroperoxide HOMs under acidic $(NH_4)HSO_4$ seed conditions.

3.6. Atmospheric Implications

HOMs formed from α-pinene/OH reactions have diverse uptake behaviors due to their different reactivities in the particle-phase. Based on the results from both online and offline measurements, it can be concluded that the reactions of hydroperoxyl HOMs can play a major role in SOA formation leading to the continuously reactive uptake of HOMs under suitable aerosol phase-state and acidity conditions. Moreover, the partitioned HOMs can further react with HSO_4^-, leading to the organosulfate formation under typical acidic aerosol particle conditions (Pye et al., 2020). With a pK_a of 1.92, HSO_4^- are abundant under more acidic particle conditions. Considering the low acidity of freshly formed particles during the early growth process, it further confirms that the HOMs uptake can play a significant role not only for the SOA formation, but also for the early growth of newly formed particles. This can have significant implications for the understanding of the atmospheric formation and processing of aerosols, as well as encourage further intense scientific investigations. Meanwhile, obtained uptake coefficients for numerous HOMs could be implemented in atmospheric chemical models. Furthermore, the present study also indicates the need to consider subsequent acidity-driven particle-phase chemistry into advanced models. All in all, this would help to gain a better understanding of atmospheric aerosol particle formation and early growth as well as enable the improvement of model SOA predictions.

4. Conclusions

In the present study, both online and offline chamber experiments were performed to explore the gas-particle uptake and subsequent particle-phase chemistry of HOMs from α-pinene/OH oxidation. Based on their contribution to the total HOMs, 39 HOMs were put into focus and their uptake behaviors were investigated. In addition, particle-phase organic mass formation was studied, and a significant acidity and/or phase state effect was observed.

During the initial uptake process, uptake coefficients γ for all the individual HOMs were derived under both seed conditions. Results showed that γ values of HOMs taken up onto Na_2SO_4 seed particles are on average 1.7 times higher than those taken up to $(NH_4)HSO_4$ seed particles. This can be attributed to the lower SSA of the Na_2SO_4 seed particles and the higher k_{1st} of HOMs under Na_2SO_4 conditions. The difference in the k_{1st} can be due to the different phase-states of the two seeds. In addition, uptake coefficients of investigated HOMs were found strongly correlated to the molar mass and also linked to their O/C ratio. Moreover, a resistance model was applied to clarify whether the experimentally determined total γ is limited by individual processes in the gas and the particle-phase. We found that the mass accommodation coefficient α is the key limiting factor for the uptake

of the most produced HOMs with a high Henry's law constant. In cases of compounds with a lower Henry's law constant H (i.e., $C_{10}H_{16}O_5$), the diffusion and reaction in bulk phase play a greater role in semi-solid particles.

All investigated closed-shell HOMs from α-pinene/OH oxidation in this study were grouped into four classes according to their different uptake behaviors. Basically, higher oxygenated HOMs with more hydroperoxyl moieties were found more reactive, and seed acidity can play a key role in the uptake process and chemical fate of HOMs in certain classes. According to their acidity-dependent reactivity, the class C HOMs appear to be the class responsible of the higher OA formation under acidic $(NH_4)HSO_4$ seed conditions.

The injection of seed particles resulted in (a) a decrease in the gas-phase HOMs concentrations and, at the same time, (b) an increase in the particle-phase OA mass concentration. Significant differences in the SOA chemical composition between the two types of seed were observed from both the online uptake experiments and the offline sample analyses. One of them is the presence of organosulfates, including HOOS, which are exclusively found on acidic $(NH_4)HSO_4$ seed. The suggested explanation is that the particle-phase organosulfate formation from HOMs via the mechanism of the nucleophilic attack of HSO_4^- is a main driver of the reactive uptake under $(NH_4)HSO_4$ seed conditions.

Data Availability Statement

The data (measured α-pinene gas-phase concentration, HOMs gas-phase concentrations, and organic, sulfate as well as ammonium particle mass concentration) used in this study are archived and available at the EUROCHAMP Data Center (https://doi.org/10.25326/FJNF-7224 [Herrmann, 2021a] and https://doi.org/10.25326/KC8N-DY53 [Herrmann, 2021b]). Data from Figure 2 and Figure S9 in Supporting Information S1 are given in Table 1. All data from Figures 3 and 5 and Figures S10 and S14 in Supporting Information S1 are available at the public data repository Zenodo (https://doi.org/10.5281/zenodo.6833062 [Poulain et al., 2022]). The estimation of the vapor pressure and Henry constants were performed by EVAPORATION (Compernolle et al., 2011) using the UManSysProp v1.0 facility, http://umansysprop.seaes.manchester.ac.uk/ (Topping et al., 2016) and HENRYWIN, https://hero.epa.gov/hero/index.cfm/reference/details/reference_id/7259635 (Meylan & Howard, 1991; US-EPA, 2012), respectively, and given in Figure S8 in Supporting Information S1. For the estimation of the contribution of different HOM loss processes (Figure S6 in Supporting Information S1), the applied OH concentration was modeled by F0AM model (https://github.com/AirChem/F0AM) using the MCM3.3.1 mechanism (Wolfe et al., 2016). Software: AMS data were analyzed with IGOR Pro 8.04 (Igor Pro, www.wavemetrics.com), API-ToF-MS data were analyzed with TofTool 5.67 (Junninen et al., 2010) under Matlab 8.3.0.532 (https://mathworks.com/products/matlab.html). Figures were made with Igor Pro 8.04, Origin Pro 2021b (https://www.originlab.com/), Sigma Plot 14 (http://www.systat.de/), and Gnuplot 5.0 (http://gnuplot.sourceforge.net/).

Acknowledgments
This study was supported by the National Natural Science Foundation of China (No. 21976108), and Horizon 2020 Projects EUROCHAMP-2020 (Grant No. 730997). Open Access funding enabled and organized by Projekt DEAL.

References

Alexander, J. M., Bell, D. M., Imre, D., Kleiber, P. D., Grassian, V. H., & Zelenyuk, A. (2016). Measurement of size-dependent dynamic shape factors of quartz particles in two flow regimes. *Aerosol Science and Technology*, *50*(8), 870–879. https://doi.org/10.1080/02786826.2016.1200006

Ammann, M., Cox, R. A., Crowley, J. N., Jenkin, M. E., Mellouki, A., Rossi, M. J., et al. (2013). Evaluated kinetic and photochemical data for atmospheric chemistry: Volume VI—Heterogeneous reactions with liquid substrates. *Atmospheric Chemistry and Physics*, *13*(16), 8045–8228. https://doi.org/10.5194/acp-13-8045-2013

Badger, C. L., George, I., Griffiths, P. T., Braban, C. F., Cox, R. A., & Abbatt, J. P. D. (2006). Phase transitions and hygroscopic growth of aerosol particles containing humic acid and mixtures of humic acid and ammonium sulfate. *Atmospheric Chemistry and Physics*, *6*(3), 755–768. https://doi.org/10.5194/acp-6-755-2006

Berndt, T., Hyttinen, N., Herrmann, H., & Hansel, A. (2019). First oxidation products from the reaction of hydroxyl radicals with isoprene for pristine environmental conditions. *Communications Chemistry*, *2*(1), 21. https://doi.org/10.1038/s42004-019-0120-9

Berndt, T., Richters, S., Jokinen, T., Hyttinen, N., Kurtén, T., Otkjær, R. V., et al. (2016). Hydroxyl radical-induced formation of highly oxidized organic compounds. *Nature Communications*, *7*(1), 13677. https://doi.org/10.1038/ncomms13677

Berndt, T., Richters, S., Kaethner, R., Voigtlaender, J., Stratmann, F., Sipilae, M., et al. (2015). Gas-phase ozonolysis of cycloalkenes: Formation of highly oxidized RO_2 radicals and their reactions with NO, NO_2, SO_2, and other RO_2 radicals. *Journal of Physical Chemistry A*, *119*(41), 10336–10348. https://doi.org/10.1021/acs.jpca.5b07295

Bianchi, F., Kurtén, T., Riva, M., Mohr, C., Rissanen, M. P., Roldin, P., et al. (2019). Highly oxygenated organic molecules (HOM) from gas-phase autoxidation involving peroxy radicals: A key contributor to atmospheric aerosol. *Chemical Reviews*, *119*(6), 3472–3509. https://doi.org/10.1021/acs.chemrev.8b00395

Brüggemann, M., Poulain, L., Held, A., Stelzer, T., Zuth, C., Richters, S., et al. (2017). Real-time detection of highly oxidized organosulfates and BSOA marker compounds during the F-BEACh 2014 field study. *Atmospheric Chemistry and Physics*, *17*(2), 1453–1469. https://doi.org/10.5194/acp-17-1453-2017

Brüggemann, M., Xu, R., Tilgner, A., Kwong, K. C., Mutzel, A., Poon, H. Y., et al. (2020). Organosulfates in ambient aerosol: State of knowledge and future research directions on formation, abundance, fate, and importance. *Environmental Science & Technology*, *54*(7), 3767–3782. https://doi.org/10.1021/acs.est.9b06751

Chen, Q., Liu, Y., Donahue, N. M., Shilling, J. E., & Martin, S. T. (2011). Particle-phase chemistry of secondary organic material: Modeled compared to measured O:C and H:C elemental ratios provide constraints. *Environmental Science & Technology*, *45*(11), 4763–4770. https://doi.org/10.1021/es104398s

Compernolle, S., Ceulemans, K., & Müller, J. F. (2011). Evaporation: A new vapor pressure estimation method for organic molecules including non-additivity and intramolecular interactions. *Atmospheric Chemistry and Physics*, *11*(18), 9431–9450. https://doi.org/10.5194/acp-11-9431-2011

Cooper, W. (1951). 1-Hydroxy cyclo hexyl 1-hydroperoxide: Its thermal decomposition and its reaction with acyl chlorides. *Journal of the Chemical Society*, *5*, 1340–1343. https://doi.org/10.1039/jr9510001340

Crounse, J. D., Nielsen, L. B., Jorgensen, S., Kjaergaard, H. G., & Wennberg, P. O. (2013). Autoxidation of organic compounds in the atmosphere. *Journal of Physical Chemistry Letters*, *4*(20), 3513–3520. https://doi.org/10.1021/jz4019207

Cziczo, D. J., Nowak, J. B., Hu, J. H., & Abbatt, J. P. D. (1997). Infrared spectroscopy of model tropospheric aerosols as a function of relative humidity: Observation of deliquescence and crystallization. *Journal of Geophysical Research: Atmospheres*, *102*(D15), 18843–18850. https://doi.org/10.1029/97jd01361

D'Ambro, E. L., Moller, K. H., Lopez-Hilfiker, F. D., Schobesberger, S., Liu, J., Shilling, J. E., et al. (2017). Isomerization of second-generation isoprene peroxy radicals: Epoxide formation and implications for secondary organic aerosol yields. *Environmental Science & Technology*, *51*(9), 4978–4987. https://doi.org/10.1021/acs.est.7b00460

DeCarlo, P. F., Kimmel, J. R., Trimborn, A., Northway, M. J., Jayne, J. T., Aiken, A. C., et al. (2006). Field-deployable, high-resolution, time-of-flight aerosol mass spectrometer. *Analytical chemistry*, *78*(24), 8281–8289. https://doi.org/10.1021/ac061249n

Donahue, N. M., Kroll, J. H., Pandis, S. N., & Robinson, A. L. (2012). A two-dimensional volatility basis set—Part 2: Diagnostics of organic-aerosol evolution. *Atmospheric Chemistry and Physics*, *12*(2), 615–634. https://doi.org/10.5194/acp-12-615-2012

Drozd, G. T., Woo, J. L., & McNeill, V. F. (2013). Self-limited uptake of alpha-pinene oxide to acidic aerosol: The effects of liquid-liquid phase separation and implications for the formation of secondary organic aerosol and organosulfates from epoxides. *Atmospheric Chemistry and Physics*, *13*(16), 8255–8263. https://doi.org/10.5194/acp-13-8255-2013

Duporté, G., Flaud, P. M., Kammer, J., Geneste, E., Augagneur, S., Pangui, E., et al. (2020). Experimental study of the formation of organosulfates from α-pinene oxidation. 2. Time evolution and effect of particle acidity. *The Journal of Physical Chemistry A*, *124*(2), 409–421. https://doi.org/10.1021/acs.jpca.9b07156

Ehn, M., Kleist, E., Junninen, H., Petäjä, T., Lonn, G., Schobesberger, S., et al. (2012). Gas phase formation of extremely oxidized pinene reaction products in chamber and ambient air. *Atmospheric Chemistry and Physics*, *12*(11), 5113–5127. https://doi.org/10.5194/acp-12-5113-2012

Ehn, M., Thornton, J. A., Kleist, E., Sipilä, M., Junninen, H., Pullinen, I., et al. (2014). A large source of low-volatility secondary organic aerosol. *Nature*, *506*(7489), 476–479. https://doi.org/10.1038/nature13032

Enami, S. (2021). Fates of organic hydroperoxides in atmospheric condensed phases. *Journal of Physical Chemistry A*, *125*(21), 4513–4523. https://doi.org/10.1021/acs.jpca.1c01513

Ervens, B., Turpin, B. J., & Weber, R. J. (2011). Secondary organic aerosol formation in cloud droplets and aqueous particles (aqSOA): A review of laboratory, field, and model studies. *Atmospheric Chemistry and Physics*, *11*(21), 11069–11102. https://doi.org/10.5194/acp-11-11069-2011

Finlayson-Pitts, B. J., & Pitts, J. N. (2000). Chapter 5—Kinetics and atmospheric chemistry. In B. J. Finlayson-Pitts, & J. N. Pitts (Eds.), *Chemistry of the upper and lower atmosphere* (pp. 130–178). Academic Press. https://doi.org/10.1016/b978-012257060-5/50007-1

Fuller, E. N., Schettler, P. D., & Giddings, J. C. (1966). A new method for prediction of binary gas-phase diffusion coefficients. *Industrial and Engineering Chemistry*, *58*(5), 18–27. https://doi.org/10.1021/ie50677a007

Gao, Y., Yu, L. E., & Chen, S. B. (2007). Efflorescence relative humidity of mixed sodium chloride and sodium sulfate particles. *Journal of Physical Chemistry A*, *111*(42), 10660–10666. https://doi.org/10.1021/jp073186y

Gaston, C. J., Riedel, T. P., Zhang, Z., Gold, A., Surratt, J. D., & Thornton, J. A. (2014). Reactive uptake of an isoprene-derived epoxydiol to submicron aerosol particles. *Environmental Science & Technology*, *48*(19), 11178–11186. https://doi.org/10.1021/es5034266

Gatzsche, K., Iinuma, Y., Mutzel, A., Berndt, T., Poulain, L., Tilgner, A., & Wolke, R. (2018). *Kinetic modeling of SOA formation for* α- and β-pinene (edited, pp. 559–564). Springer International Publishing. https://doi.org/10.1007/978-3-319-57645-9_87

Gill, K. J., & Hites, R. A. (2002). Rate constants for the gas-phase reactions of the hydroxyl radical with isoprene, α- and β-pinene, and limonene as a function of temperature. *The Journal of Physical Chemistry A*, *106*(11), 2538–2544. https://doi.org/10.1021/jp013532q

Goldstein, A. H., & Galbally, I. E. (2007). Known and unexplored organic constituents in the earth's atmosphere. *Environmental Science & Technology*, *41*(5), 1514–1521. https://doi.org/10.1021/es072476p

Hallquist, M., Wenger, J. C., Baltensperger, U., Rudich, Y., Simpson, D., Claeys, M., et al. (2009). The formation, properties, and impact of secondary organic aerosol: Current and emerging issues. *Atmospheric Chemistry and Physics*, *9*(14), 5155–5236. https://doi.org/10.5194/acp-9-5155-2009

Herrmann, H. (2021a). Atmospheric simulation chamber study: Alpha-pinene + OH - Aerosol study - heterogeneous reactivity. [Dataset]. AERIS. https://doi.org/10.25326/FJNF-7224

Herrmann, H. (2021b). Atmospheric simulation chamber study: Alpha-pinene + OH - Aerosol study - heterogeneous reactivity. [Dataset]. AERIS. https://doi.org/10.25326/KC8N-DY53

Herrmann, H., Schaefer, T., Tilgner, A., Styler, S., Weller, C., Teich, M., & Otto, T. (2015). Tropospheric aqueous-phase chemistry: Kinetics, mechanisms, and its coupling to a changing gas phase. *Chemical Reviews*, *115*, 4259–4334. https://doi.org/10.1021/cr500447k

Hettiyadura, A. P. S., Al-Naiema, I. M., Hughes, D. D., Fang, T., & Stone, E. A. (2019). Organosulfates in Atlanta, Georgia: Anthropogenic influences on biogenic secondary organic aerosol formation. *Atmospheric Chemistry and Physics*, *19*(5), 3191–3206. https://doi.org/10.5194/acp-19-3191-2019

Hettiyadura, A. P. S., Jayarathne, T., Baumann, K., Goldstein, A. H., de Gouw, J. A., Koss, A., et al. (2017). Qualitative and quantitative analysis of atmospheric organosulfates in Centreville, Alabama. *Atmospheric Chemistry and Physics*, *17*(2), 1343–1359. https://doi.org/10.5194/acp-17-1343-2017

Hock, H., & Lang, S. (1944). Autoxydation von kohlenwasserstoffen, IX. mitteil.: Über peroxyde von benzol-derivaten. *Berichte der Deutschen Chemischen Gesellschaft*, *77*(3–4), 257–264. https://doi.org/10.1002/cber.19440770321

Hodzic, A., Kasibhatla, P. S., Jo, D. S., Cappa, C. D., Jimenez, J. L., Madronich, S., & Park, R. J. (2016). Rethinking the global secondary organic aerosol (SOA) budget: Stronger production, faster removal, shorter lifetime. *Atmospheric Chemistry and Physics*, *16*(12), 7917–7941. https://doi.org/10.5194/acp-16-7917-2016

Huang, W., Li, H., Sarnela, N., Heikkinen, L., Tham, Y. J., Mikkilä, J., et al. (2021). Measurement report: Molecular composition and volatility of gaseous organic compounds in a boreal forest—From volatile organic compounds to highly oxygenated organic molecules. *Atmospheric Chemistry and Physics*, *21*(11), 8961–8977. https://doi.org/10.5194/acp-21-8961-2021

Iinuma, Y., Böge, O., Kahnt, A., & Herrmann, H. (2009). Laboratory chamber studies on the formation of organosulfates from reactive uptake of monoterpene oxides. *Physical Chemistry Chemical Physics*, *11*(36), 7985–7997. https://doi.org/10.1039/B904025K

Jimenez, J. L., Canagaratna, M. R., Donahue, N. M., Prevot, A. S. H., Zhang, Q., Kroll, J. H., et al. (2009). Evolution of organic aerosols in the atmosphere. *Science*, *326*(5959), 1525–1529. https://doi.org/10.1126/science.1180353

Jokinen, T., Berndt, T., Makkonen, R., Kerminen, V.-M., Junninen, H., Paasonen, P., et al. (2015). Production of extremely low volatile organic compounds from biogenic emissions: Measured yields and atmospheric implications. *Proceedings of the National Academy of Sciences of the United States of America*, *112*(23), 7123–7128. https://doi.org/10.1073/pnas.1423977112

Jokinen, T., Sipilä, M., Richters, S., Kerminen, V.-M., Paasonen, P., Stratmann, F., et al. (2014). Rapid autoxidation forms highly oxidized RO_2 radicals in the atmosphere. *Angewandte Chemie-International Edition*, *53*(52), 14596–14600. https://doi.org/10.1002/anie.201408566

Junninen, H., Ehn, M., Petäjä, T., Luosujärvi, L., Kotiaho, T., Kostiainen, R., et al. (2010). A high-resolution mass spectrometer to measure atmospheric ion composition. *Atmospheric Measurement Techniques*, *3*(4), 1039–1053. https://doi.org/10.5194/amt-3-1039-2010

Krapf, M., El Haddad, I., Bruns, E. A., Molteni, U., Daellenbach, K. R., Prevot, A. S. H., et al. (2016). Labile peroxides in secondary organic aerosol. *Chem*, *1*(4), 603–616. https://doi.org/10.1016/j.chempr.2016.09.007

Kristensen, K., Jensen, L. N., Quéléver, L. L. J., Christiansen, S., Rosati, B., Elm, J., et al. (2020). The Aarhus Chamber Campaign on Highly oxygenated organic molecules and Aerosols (ACCHA): Particle formation, organic acids, and dimer esters from α-pinene ozonolysis at different temperatures. *Atmospheric Chemistry and Physics*, *20*(21), 12549–12567. https://doi.org/10.5194/acp-20-12549-2020

Kürten, A., Bergen, A., Heinritzi, M., Leiminger, M., Lorenz, V., Piel, F., et al. (2016). Observation of new particle formation and measurement of sulfuric acid, ammonia, amines, and highly oxidized organic molecules at a rural site in central Germany. *Atmospheric Chemistry and Physics*, *16*(19), 12793–12813. https://doi.org/10.5194/acp-16-12793-2016

Lal, V., Khalizov, A. F., Lin, Y., Galvan, M. D., Connell, B. T., & Zhang, R. (2012). Heterogeneous reactions of epoxides in acidic media. *Journal of Physical Chemistry A*, *116*(24), 6078–6090. https://doi.org/10.1021/jp2112704

Li, H., Chen, Z. M., Huang, L. B., & Huang, D. (2016). Organic peroxides' gas-particle partitioning and rapid heterogeneous decomposition on secondary organic aerosol. *Atmospheric Chemistry and Physics*, *16*(3), 1837–1848. https://doi.org/10.5194/acp-16-1837-2016

Liu, X., Day, D. A., Krechmer, J. E., Brown, W., Peng, Z., Ziemann, P. J., & Jimenez, J. L. (2019). Direct measurements of semi-volatile organic compound dynamics show near-unity mass accommodation coefficients for diverse aerosols. *Communications Chemistry*, *2*(1), 98. https://doi.org/10.1038/s42004-019-0200-x

Mennola, T., Noponen, M., Aronniemi, M., Hottinen, T., Mikkola, M., Himanen, O., & Lund, P. (2003). Mass transport in the cathode of a free-breathing polymer electrolyte membrane fuel cell. *Journal of Applied Electrochemistry*, *33*(11), 979–987. https://doi.org/10.1023/a:1026279431097

Mentel, T. F., Springer, M., Ehn, M., Kleist, E., Pullinen, I., Kurtén, T., et al. (2015). Formation of highly oxidized multifunctional compounds: Autoxidation of peroxy radicals formed in the ozonolysis of alkenes—Deduced from structure-product relationships. *Atmospheric Chemistry and Physics*, *15*(12), 6745–6765. https://doi.org/10.5194/acp-15-6745-2015

Meylan, W. M., & Howard, P. H. (1991). Bond contribution method for estimating Henry's law constants. *Environmental Toxicology and Chemistry*, *10*(10), 1283–1293. https://doi.org/10.1002/etc.5620101007

Minerath, E. C., & Elrod, M. J. (2009). Assessing the potential for diol and hydroxy sulfate ester formation from the reaction of epoxides in tropospheric aerosols. *Environmental Science & Technology*, *43*(5), 1386–1392. https://doi.org/10.1021/es8029076

Mutzel, A., Poulain, L., Berndt, T., Iinuma, Y., Rodigast, M., Böge, O., et al. (2015). Highly oxidized multifunctional organic compounds observed in tropospheric particles: A field and laboratory study. *Environmental Science & Technology*, *49*(13), 7754–7761. https://doi.org/10.1021/acs.est.5b00885

Mutzel, A., Rodigast, M., Iinuma, Y., Böge, O., & Herrmann, H. (2016). Monoterpene SOA—Contribution of first-generation oxidation products to formation and chemical composition. *Atmospheric Environment*, *130*, 136–144. https://doi.org/10.1016/j.atmosenv.2015.10.080

Nguyen, T. B., Coggon, M. M., Bates, K. H., Zhang, X., Schwantes, R. H., Schilling, K. A., et al. (2014). Organic aerosol formation from the reactive uptake of isoprene epoxydiols (IEPOX) onto non-acidified inorganic seeds. *Atmospheric Chemistry and Physics*, *14*(7), 3497–3510. https://doi.org/10.5194/acp-14-3497-2014

O'Sullivan, D. W., Lee, M. Y., Noone, B. C., & Heikes, B. G. (1996). Henry's law constant determinations for hydrogen peroxide, methyl hydroperoxide, hydroxymethyl hydroperoxide, ethyl hydroperoxide, and peroxyacetic acid. *Journal of Physical Chemistry*, *100*(8), 3241–3247. https://doi.org/10.1021/jp951168n

Pai, S. J., Heald, C. L., Pierce, J. R., Farina, S. C., Marais, E. A., Jimenez, J. L., et al. (2020). An evaluation of global organic aerosol schemes using airborne observations. *Atmospheric Chemistry and Physics*, *20*(5), 2637–2665. https://doi.org/10.5194/acp-20-2637-2020

Peräkylä, O., Riva, M., Heikkinen, L., Quéléver, L., Roldin, P., & Ehn, M. (2020). Experimental investigation into the volatilities of highly oxygenated organic molecules (HOMs). *Atmospheric Chemistry and Physics*, *20*(2), 649–669. https://doi.org/10.5194/acp-20-649-2020

Pospisilova, V., Bell, D. M., Lamkaddam, H., Bertrand, A., Wang, L., Bhattu, D., et al. (2021). Photodegradation of alpha-pinene secondary organic aerosol dominated by moderately oxidized molecules. *Environmental Science & Technology*, *55*(10), 6936–6943. https://doi.org/10.1021/acs.est.0c06752

Poulain, L., Tilgner, A., Brüggemann, M., Mettke, P., He, L., Anders, J., et al. (2022). Particle-Phase Uptake and Chemistry of Highly Oxygenated Organic Molecules (HOMs) from α-Pinene OH Oxidation. [Dataset]. Zenodo. https://doi.org/10.5281/zenodo.6833062

Praplan, A. P., Schobesberger, S., Bianchi, F., Rissanen, M. P., Ehn, M., Jokinen, T., et al. (2015). Elemental composition and clustering behavior of α -pinene oxidation products for different oxidation conditions. *Atmospheric Chemistry and Physics*, *15*(8), 4145–4159. https://doi.org/10.5194/acp-15-4145-2015

Pye, H. O. T., Nenes, A., Alexander, B., Ault, A. P., Barth, M. C., Clegg, S. L., et al. (2020). The acidity of atmospheric particles and clouds. *Atmospheric Chemistry and Physics*, *20*(8), 4809–4888. https://doi.org/10.5194/acp-20-4809-2020

Rissanen, M. P., Kurtén, T., Sipilä, M., Thornton, J. A., Kangasluoma, J., Sarnela, N., et al. (2014). The formation of highly oxidized multifunctional products in the ozonolysis of cyclohexene. *Journal of the American Chemical Society*, *136*(44), 15596–15606. https://doi.org/10.1021/ja507146s

Riva, M., Budisulistiorini, S. H., Chen, Y. Z., Zhang, Z. F., D'Ambro, E. L., Zhang, X., et al. (2016). Chemical characterization of secondary organic aerosol from oxidation of isoprene hydroxyhydroperoxides. *Environmental Science & Technology*, *50*(18), 9889–9899. https://doi.org/10.1021/acs.est.6b02511

Riva, M., Budisulistiorini, S. H., Zhang, Z. F., Gold, A., Thornton, J. A., Turpin, B. J., & Surratt, J. D. (2017). Multiphase reactivity of gaseous hydroperoxide oligomers produced from isoprene ozonolysis in the presence of acidified aerosols. *Atmospheric Environment*, *152*, 314–322. https://doi.org/10.1016/j.atmosenv.2016.12.040

Riva, M., Heikkinen, L., Bell, D. M., Peräkylä, O., Zha, Q., Schallhart, S., et al. (2019). Chemical transformations in monoterpene-derived organic aerosol enhanced by inorganic composition. *npj Climate and Atmospheric Science*, *2*(1), 1–9. https://doi.org/10.1038/s41612-018-0058-0

Roldin, P., Ehn, M., Kurtén, T., Olenius, T., Rissanen, M. P., Sarnela, N., et al. (2019). The role of highly oxygenated organic molecules in the Boreal aerosol-cloud-climate system. *Nature Communications*, *10*(1), 4370. https://doi.org/10.1038/s41467-019-12338-8

Schwartz, S. E. (1986). Mass-transport considerations pertinent to aqueous phase reactions of gases in liquid-water clouds. In *Chemistry of multiphase atmospheric systems* (edited, pp. 415–471). NATO. https://doi.org/10.1007/978-3-642-70627-1_16

Shrivastava, M., Easter, R. C., Liu, X., Zelenyuk, A., Singh, B., Zhang, K., et al. (2015). Global transformation and fate of SOA: Implications of low-volatility SOA and gas-phase fragmentation reactions. *Journal of Geophysical Research: Atmospheres*, *120*(9), 4169–4195. https://doi.org/10.1002/2014jd022563

Spracklen, D. V., Jimenez, J. L., Carslaw, K. S., Worsnop, D. R., Evans, M. J., Mann, G. W., et al. (2011). Aerosol mass spectrometer constraint on the global secondary organic aerosol budget. *Atmospheric Chemistry and Physics*, *11*(23), 12109–12136. https://doi.org/10.5194/acp-11-12109-2011

Staffelbach, T. A., & Kok, G. L. (1993). Henry's law constants for aqueous solutions of hydrogen peroxide and hydroxymethyl hydroperoxide. *Journal of Geophysical Research-Atmospheres*, *98*(D7), 12713–12717. https://doi.org/10.1029/93jd01022

Surratt, J. D., Chan, A. W. H., Eddingsaas, N. C., Chan, M. N., Loza, C. L., Kwan, A. J., et al. (2010). Reactive intermediates revealed in secondary organic aerosol formation from isoprene. *Proceedings of the National Academy of Sciences of the United States of America*, *107*(15), 6640–6645. https://doi.org/10.1073/pnas.0911114107

Surratt, J. D., Gómez-González, Y., Chan, A. W. H., Vermeylen, R., Shahgholi, M., Kleindienst, T. E., et al. (2008). Organosulfate formation in biogenic secondary organic aerosol. *Journal of Physical Chemistry A*, *112*(36), 8345–8378. https://doi.org/10.1021/jp802310p

Surratt, J. D., Kroll, J. H., Kleindienst, T. E., Edney, E. O., Claeys, M., Sorooshian, A., et al. (2007). Evidence for organosulfates in secondary organic aerosol. *Environmental Science & Technology*, *41*(2), 517–527. https://doi.org/10.1021/es062081q

Tang, I. N., & Munkelwitz, H. R. (1994). Water activities, densities, and refractive-indexes of aqueous sulfates and sodium-nitrate droplets of atmospheric importance. *Journal of Geophysical Research: Atmospheres*, *99*(D9), 18801–18808. https://doi.org/10.1029/94jd01345

Tilgner, A., Schaefer, T., Alexander, B., Barth, M., Collett, J. L., Jr., Fahey, K. M., et al. (2021). Acidity and the multiphase chemistry of atmospheric aqueous particles and clouds. *Atmospheric Chemistry and Physics*, *21*(17), 13483–13536. https://doi.org/10.5194/acp-21-13483-2021

Tomaz, S., Wang, D., Zabalegui, N., Li, D., Lamkaddam, H., Bachmeier, F., et al. (2021). Structures and reactivity of peroxy radicals and dimeric products revealed by online tandem mass spectrometry. *Nature Communications*, *12*(1), 300. https://doi.org/10.1038/s41467-020-20532-2

Tong, H., Liu, F., Filippi, A., Wilson, J., Arangio, A. M., Zhang, Y., et al. (2021). Aqueous-phase reactive species formed by fine particulate matter from remote forests and polluted urban air. *Atmospheric Chemistry and Physics*, *21*(13), 10439–10455. https://doi.org/10.5194/acp-21-10439-2021

Tong, H., Zhang, Y., Filippi, A., Wang, T., Li, C., Liu, F., et al. (2019). Radical formation by fine particulate matter associated with highly oxygenated molecules. *Environmental Science & Technology*, *53*(21), 12506–12518. https://doi.org/10.1021/acs.est.9b05149

Topping, D., Barley, M., Bane, M. K., Higham, N., Aumont, B., Dingle, N., & McFiggans, G. (2016). UManSysProp v1.0: An online and open-source facility for molecular property prediction and atmospheric aerosol calculations. *Geoscientific Model Development*, *9*(2), 899–914. https://doi.org/10.5194/gmd-9-899-2016

Tröstl, J., Chuang, W. K., Gordon, H., Heinritzi, M., Yan, C., Molteni, U., et al. (2016). The role of low-volatility organic compounds in initial particle growth in the atmosphere. *Nature*, *533*(7604), 527–531. https://doi.org/10.1038/nature18271

Tsigaridis, K., Daskalakis, N., Kanakidou, M., Adams, P. J., Artaxo, P., Bahadur, R., et al. (2014). The AeroCom evaluation and intercomparison of organic aerosol in global models. *Atmospheric Chemistry and Physics*, *14*(19), 10845–10895. https://doi.org/10.5194/acp-14-10845-2014

Tsigaridis, K., & Kanakidou, M. (2018). The present and future of secondary organic aerosol direct forcing on climate. *Current Climate Change Reports*, *4*(2), 84–98. https://doi.org/10.1007/s40641-018-0092-3

US-EPA. (2012). *Estimation Programs Interface Suite™ for Microsoft® Windows, v 4.11*. United States Environmental Protection Agency.

Vereecken, L., & Nozière, B. (2020). H migration in peroxy radicals under atmospheric conditions. *Atmospheric Chemistry and Physics*, *20*(12), 7429–7458. https://doi.org/10.5194/acp-20-7429-2020

von Sonntag, C., & Schuchmann, H. P. (1991). The elucidation of peroxyl radical reactions in aqueous solution with the help of radiation-chemical methods. *Angewandte Chemie-International Edition in English*, *30*(10), 1229–1253. https://doi.org/10.1002/anie.199112291

Wang, Z., Ehn, M., Rissanen, M. P., Garmash, O., Quéléver, L., Xing, L., et al. (2021). Efficient alkane oxidation under combustion engine and atmospheric conditions. *Communications Chemistry*, *4*(1), 18. https://doi.org/10.1038/s42004-020-00445-3

Wiedensohler, A., Birmili, W., Nowak, A., Sonntag, A., Weinhold, K., Merkel, M., et al. (2012). Mobility particle size spectrometers: Harmonization of technical standards and data structure to facilitate high-quality long-term observations of atmospheric particle number size distributions. *Atmospheric Measurement Techniques*, *5*(3), 657–685. https://doi.org/10.5194/amt-5-657-2012

Wolfe, G. M., Marvin, M. R., Roberts, S. J., Travis, K. R., & Liao, J. (2016). The framework for 0-D atmospheric modeling (F0AM) v3.1. *Geoscientific Model Development*, *9*(9), 3309–3319. https://doi.org/10.5194/gmd-9-3309-2016

Wong, J. P., Zhou, S., & Abbatt, J. P. (2015). Changes in secondary organic aerosol composition and mass due to photolysis: Relative humidity dependence. *Journal of Physical Chemistry A*, *119*(19), 4309–4316. https://doi.org/10.1021/jp506898c

Zhang, Q., Jimenez, J. L., Canagaratna, M. R., Allan, J. D., Coe, H., Ulbrich, I., et al. (2007). Ubiquity and dominance of oxygenated species in organic aerosols in anthropogenically influenced northern hemisphere midlatitudes. *Geophysical Research Letters*, *34*(13), L13801. https://doi.org/10.1029/2007gl029979

Zhang, X., Lambe, A. T., Upshur, M. A., Brooks, W. A., Gray Bé, A., Thomson, R. J., et al. (2017). Highly oxygenated multifunctional compounds in α-pinene secondary organic aerosol. *Environmental Science & Technology*, *51*(11), 5932–5940. https://doi.org/10.1021/acs.est.6b06588

Zhang, Y., Chen, Y., Lambe, A. T., Olson, N. E., Lei, Z., Craig, R. L., et al. (2018). Effect of the aerosol-phase state on secondary organic aerosol formation from the reactive uptake of isoprene-derived epoxydiols (IEPOX). *Environmental Science and Technology Letters*, *5*(3), 167–174. https://doi.org/10.1021/acs.estlett.8b00044

Zhao, J., Ortega, J., Chen, M., McMurry, P. H., & Smith, J. N. (2013). Dependence of particle nucleation and growth on high-molecular-weight gas-phase products during ozonolysis of α-pinene. *Atmospheric Chemistry and Physics*, *13*(15), 7631–7644. https://doi.org/10.5194/acp-13-7631-2013

Zhao, R., Lee, A. K. Y., Soong, R., Simpson, A. J., & Abbatt, J. P. D. (2013). Formation of aqueous-phase α-hydroxyhydroperoxides (α-HHP): Potential atmospheric impacts. *Atmospheric Chemistry and Physics*, *13*(12), 5857–5872. https://doi.org/10.5194/acp-13-5857-2013

Zhou, X. L., & Lee, Y. N. (1992). Aqueous solubility and reaction kinetics of hydroxymethyl hydroperoxide. *Journal of Physical Chemistry*, *96*(1), 265–272. https://doi.org/10.1021/j100180a051

References From the Supporting Information

Mettke, P., Mutzel, A., Böge, O., & Herrmann, H. (2022). Synthesis and characterization of atmospherically relevant hydroxy hydroperoxides. *Atmosphere*, *13*(4), 1–19. https://doi.org/10.3390/atmos13040507

Zhang, Q., Canagaratna, M. R., Jayne, J. T., Worsnop, D. R., & Jimenez, J. L. (2005). Time- and size-resolved chemical composition of submicron particles in Pittsburgh: Implications for aerosol sources and processes. *Journal of Geophysical Research: Atmospheres*, *110*(D7), D07s09. https://doi.org/10.1029/2004jd004649